PHILOSOPHICAL TRANSACTIONS OF THE ROYAL SOCIETY A MATHEMATICAL, PHYSICAL & ENGINEERING SCIENCES

Computer simulation of marine ice accretion

Edward P. Lozowski, Krzysztof Szilder and Lasse Makkonen

Phil. Trans. R. Soc. Lond. A 2000 **358**, 2811-2845
doi: 10.1098/rsta.2000.0687

10.1098/rsta.2000.0687

THE ROYAL SOCIETY

Computer simulation of marine ice accretion

By Edward P. Lozowski[1], Krzysztof Szilder[2] and Lasse Makkonen[3]

[1]*Department of Earth and Atmospheric Sciences, University of Alberta, Edmonton, Alberta, Canada T6G 2E3*
[2]*Department of Civil Engineering, Kitami Institute of Technology, 165 Koen-cho, Kitami 090, Japan*
[3]*Technical Research Centre of Finland, Laboratory of Structural Engineering, Betonimiehenkuja 3, SF-02150, Espoo, Finland*

Marine icing can arguably be considered to be the primogenitor of icing problems, having occasioned grief to mariners long before aircraft or electrical transmission lines were invented. Adopting an historical perspective, we elucidate the nature of the phenomenon and the scientific and engineering approaches which have been embraced to mitigate it. With a view to encouraging other scientists to address this problem, we also identify the critical knowledge gaps which stand in the way of a final solution, paying particular attention to recent developments and future trends in numerical modelling and wind-tunnel experimentation.

Keywords: ice; accretion; marine engineering simulation; numerical model

1. Introduction

(*a*) *Background*

The effect of vessel icing on shipping, the fishery and offshore exploration and production has been well documented (Shellard 1974; Panov 1978; Chung & Lozowski 1996). Over the past 40 years or so, hundreds of papers have been published on marine icing (Lozowski & Makkonen 2001). Despite this research activity, only limited countermeasures to superstructure ice accretion have been developed (MIL Systems 1993). As a result, much reliance has been placed on marine icing forecasting, so that the operators and crews of vessels can be alerted to the potential danger and can take appropriate precautionary measures, including avoidance.

The first marine icing forecasting techniques were simple algorithms, based on statistical relations between the severity of icing and environmental conditions. These algorithms were typically formulated as nomograms (Mertins 1968; Wise & Comiskey 1980). More recently, physical models of marine icing have been developed, which were run initially on mainframe computers, but can now be run efficiently on a personal computer. These models can be used for research and design purposes, as well as for forecasting.

In this paper, we will briefly review the history of marine icing model development and describe in some detail two new approaches to superstructure icing modelling that have been developed at the University of Alberta.

(*b*) *The nature of marine ice accretion*

There are a number of forms of ice accretion that can occur at sea. These arise from the freezing and adhesion to a vessel of supercooled fog, freezing rain, snow and various types of spray. It is generally conceded that the most severe icing arises from the freezing of spray generated by vessel–wave interaction. The models we will describe here will therefore focus on spray icing.

In many respects, marine ice accretions are similar to other types of ice accretion, including hail, aircraft icing and transmission line icing. The ice growth is controlled largely by the rate of impingement of spray and the external heat transfer. Typically they all exhibit rough surfaces and may contain substantial liquid inclusions (up to *ca.* 50% by mass). In a number of ways, however, they are quite distinct from other types of accretion. First, they are formed from brine, and this affects such relevant physical variables as freezing point, equilibrium vapour pressure, viscosity and surface tension. Second, marine ice accretions may grow to be much larger than their aircraft or hail counterparts. This is a particularly important consideration because it means that the underlying geometry of the vessel has an influence on the morphology of large marine ice accretions, which diminishes with time. Although this may also be true for other types of ice accretion, particularly rime ice accretions on mountain tops (C. C. Ryerson, personal communication), the effect is generally not so pronounced for transmission lines, where even large ice or wet snow accretions tend to remain cylindrical due to rotation of the wire. Finally, marine ice accretions are generally wet, leading to the formation of roughness lobes, icicles and pendant ice masses.

Another distinguishing characteristic of marine icing has to do with the impinging liquid. In aircraft icing and certain types of transmission line icing, the impinging liquid consists of supercooled cloud droplets, typically tens of micrometres in diameter, that are generally assumed to be close to the air temperature. In marine icing, the impinging drops are typically one to two orders of magnitude larger (Ryerson 1995) and they arise from the sea surface, with the result that their temperature usually lies between the sea-surface temperature and the air temperature. Thus their temperature at impingement will depend on where they strike the vessel. If nucleation occurs in the droplets while in the air, they may impinge as partly frozen particles at a temperature close to their freezing point. In this respect, marine spray icing is somewhat analogous to icing under freezing rain conditions.

(*c*) *Scope of the paper*

The remainder of the paper is divided into four main sections. Section 2 provides a brief history of marine icing computer models, § 3 a detailed discussion of the United States Coast Guard Cutter (USCGC) *Midgett* model, a three-dimensional time-dependent vessel-icing model, developed at the University of Alberta, § 4 a discussion of heretofore unpublished work on the modelling of spraying for offshore rigs, and § 5 an overview of a novel approach to the modelling of large wet-ice accretions, which we refer to as morphogenetic modelling.

2. A brief history of marine-icing computer models

Because there are several review papers extant that deal in part with the early history of computer models of marine icing, this review will necessarily be brief. For

more details, the reader is referred to the work of Jessup (1985), Lozowski (1988), Makkonen (1988*b*), Lozowski & Gates (1991), Zakrzewski & Lozowski (1991) and Lozowski & Makkonen (2001).

One of the earliest physically based models, used for forecasting marine icing, was that of Borisenkov (1969). He considered freshwater icing on a cylinder and assumed that the icing rate is determined by the convective heat transfer, both sensible and evaporative, from the icing surface. Borisenkov's icing rate formula has been widely cited by subsequent investigators. Makkonen (1984), however, has pointed out a significant error in its formulation. Moreover, it ignores the sensible heat of the impinging spray, which can be quite significant (Lozowski *et al*. 1996), radiative heat transfer and salinity effects, so that its further use cannot be recommended.

In the same year, Kachurin & Gashin (1969) published a more complete theory of ship icing, also using a cylinder as the reference object. This work was derived from earlier aircraft icing theory (Kachurin 1962; Kachurin & Morachevskii 1965). Included in the theory are a number of important elements, not considered by Borisenkov, such as the influence of the liquid film on heat transfer, the effect of salinity and the heat transfer associated with the impinging and run-off liquid. In addition, in order to calculate the last of these terms, these investigators also considered the effect of wave height on spray generation and the cooling of spray droplets in flight. Finally, they made an empirical connection between the iceload prediction of the cylindrical model and the observed iceloads on research vessels. The resulting forecasting tool was published in the form of a nomogram (Kachurin *et al*. 1974). Makkonen (1988*b*) has pointed out an error in the Kachurin nomogram, related to the effect of salinity. The error has been acknowledged by Kachurin. Godard (1977) offered two computational approaches to solving the Kachurin model—the first a direct numerical solution of the equations, and the second a five-dimensional numerical interpolation of the nomogram. Stallabrass (1979) argued that the Kachurin model is too complex, given the large uncertainties in our physical understanding and the data. Consequently, he devised a simpler numerical model of marine icing on a cylinder and calibrated it with Canadian icing observations.

Makkonen (1987) presented a model of salt entrapment in spray ice and incorporated it into a cylinder icing model. The convective heat transfer coefficient in this model is calculated using a separate numerical boundary-layer model of heat transfer from a rough cylinder (Makkonen 1985). Recently, Blackmore & Lozowski (1998) have developed a theoretical model of freshwater spongy spray icing on a vertical cylinder, including a consideration of the surficial morphology beneath a falling supercooled liquid film, and the resulting entrapment of unfrozen liquid in the dendritic ice matrix. This model, however, does not yet include salinity effects.

A rather different approach to the modelling of vessel icing has been taken by Blackmore & Lozowski (1994). Their model emphasizes the heat transfer between the spray and the airstream, rather than the heat transfer between the icing surface and the airstream. Hence it is applied directly to a vessel, rather than through a correlation between simulated cylinder icing and observed vessel icing. This model is simple to program, adaptable to vessels of different size and performs as well as the Kachurin model, when tested against observations.

Horjen & Vefsnmo (1985), Horjen (1990) and Horjen & Carstens (1990) have also described a marine icing model applicable to ships. They have detailed the model

in numerous other publications, which, unfortunately, are mostly to be found in the proprietary literature.

A parallel development of marine icing models applicable to offshore drilling vessels has also occurred since the early 1980s, the impetus being the exploration and development of hydrocarbon resources in the North Sea and off the Canadian east coast. While for geometrical reasons, these models differ in detail from ship icing models, much of the underlying physics is the same. To the best of our knowledge, there are four such models extant. These are the Ashcroft (1985) model, the Romagnoli (1988) model, the RIGICE model (Roebber & Mitten 1987; Mitten 1994) and the ICEMOD model (Horjen & Vefsnmo 1986*a*,*b*, 1987; Horjen *et al*. 1988). Chung & Lozowski (1996) have recently reviewed the drilling platform icing problem, and discuss RIGICE and ICEMOD. We will say more about these latter two models, particularly RIGICE, in § 4 below.

3. A three-dimensional time-dependent vessel-icing model

In the late 1980s, Zakrzewski and colleagues published several papers on the spraying of ships (Zakrzewski 1987; Zakrzewski & Lozowski 1987; Zakrzewski *et al*. 1988). Using these models to predict the spray flux impinging onto various components of the vessel, it became possible, in principle, to construct a more complete vessel-icing model. Unlike previous models, such a model would be capable of predicting the iceload distribution over the ship. This is an important consideration for seakeeping, safety and stability. By its very nature, such a model would be vessel specific and it could readily be made time dependent in the sense of responding to changing environmental conditions.

The report by Lozowski & Zakrzewski (1993) describes the details of the first such model, developed for the USCGC *Midgett*, a high endurance coast guard patrol vessel. Subsequently, Chung & Lozowski (1999) improved the methodology, developing an icing model for the Canadian fishing trawler, MV *Zandberg*. Chung and his colleagues incorporated a new approach to spray prediction, based on an analysis of model spraying experiments in the towing tank of the Institute for Marine Dynamics, National Research Council Canada. They also introduced a simpler grid-cell discretization of the vessel surface that permitted graphical visualization of the ice-accretion distribution over the vessel. Because the spraying component of the USCGC *Midgett* model is adaptable to other vessels, while that for the *Zandberg* model is not, we choose to describe the USCGC *Midgett* model here in some detail.

(*a*) *Model structure*

First, the ship surface was divided into four general areas in which ice accretion is a concern (ahead of the main superstructure, the superstructure, the masts and antennae and the decks). Within these areas, a total of 46 icing targets were identified, such as the 'foregun on the forecastle deck', the 'hurricane bow' and so on. The targets were then subdivided into a total of 145 components, and the components in turn were discretized into a total of 1381 grid cells.

The model itself consists of four basic modules: a text-based user interface for the selection of targets and the input of environmental parameters; a spray generation

and spray trajectory module; an ice growth module and an output module. The output at each forecasting time-step (typically hourly) consists of the iceload, thickness and centre of gravity for each component, and for the entire vessel. The required model input consists of: air temperature; dewpoint temperature; air pressure; true or apparent wind speed and direction; sea-surface temperature; sea-surface salinity; fetch; ship speed; and course.

The model computes the ice accretion resulting from a single spraying event for each forecasting time-step. The total accumulated ice accretion is then determined by multiplying by the number of spraying events during the time-step. Because environmental conditions may change from one forecasting time-step to the next, the icing computations are repeated at each forecasting time-step, with the iceloads being accumulated.

In the model, the ship is allowed only one degree of freedom, namely forward translation. Possible effects on splashing of pitch, roll, yaw, heave, surge and sway are ignored. Feedback between the ice accumulation and the ship dynamics is also ignored. Chung *et al*. (1995) succeeded in taking this feedback into account for the *Zandberg* model, but only with enormous computational effort.

(*b*) *Algorithms for model physics*

(i) *Representation of the seaway*

It is assumed that the ship moves in regular seas, and that each wave encounter that leads to splashing is identical, during a particular forecasting time-step. The ocean is assumed to be deep, with a fully developed wave field, characterized by the significant wave. The significant wave height, H_s, and period, T_s, are calculated from the fetch, using fifth-degree polynomials fitted by Zakrzewski (1987) to significant wave height and period data in the Handbook of Oceanographic Tables (Bialek 1966).

(ii) *The spray jet*

The ship–wave interaction is envisaged to give rise to a spray jet in the form of a thin liquid sheet that emerges from a portion of the forward perimeter of the ship. At the initial time, it is assumed that this jet has already broken up into spray droplets of uniform size and that the liquid water concentration (LWC) of the spray cloud varies only with height. The jet is taken to be at rest initially, in a frame of reference moving forward with the ship. The motion of the droplets in the spray cloud is determined by solving the equation of motion for a single droplet. No allowance is made for variation of the wind with height, or for deflection of the airflow by the ship. Since all the droplets are assumed to be identical, their trajectories are therefore congruent.

In order to determine the spray flux to a particular grid cell, the droplet trajectory is projected backwards (upwind) from the centre of the grid cell, until it intercepts (or fails to intercept) the spray jet. If it does not intercept the jet, that grid cell remains dry and no ice accumulates during that forecasting time-step. Should the reverse trajectory intercept the spray jet, the liquid flux impinging onto the grid cell is the product of the normal component of the droplet impact speed and the LWC at the point of origin of the trajectory in the spray jet.

The vertical distribution of LWC in the spray jet, $w(z)$, is that proposed by Zakrzewski (1987),

$$w = 6.46 \times 10^{-5} H_{\mathrm{s}} v_{\mathrm{sw}}^2 \exp\left(-\frac{z}{1.82}\right), \tag{3.1}$$

where H_{s} is the significant wave height and v_{sw} is the ship speed relative to the waves. SI units will be used, unless otherwise stated, so that w is in kg m^{-3}.

The ship geometry is specified in a Cartesian coordinate system, with the z-axis vertically up, the x-axis parallel to the vessel's centreline and directed from bow to stern, and the y-axis pointing from port to starboard. The spray jet dimensions are based on the work of Zakrzewski *et al.* (1988) for a fishing trawler, with modifications to allow for the larger size of the USCGC *Midgett*. The spray jet begins at the bow ($x = 0$) and extends symmetrically along both sides of the vessel to a position, x_{e}, given by

$$x_{\mathrm{e}} = 2.0 H_{\mathrm{s}} + 0.04 v_{\mathrm{sw}}^2 - 10.0. \tag{3.2}$$

If x_{e} is negative, there is no spray jet. It should be noted that the assumed spray jet symmetry does not necessarily imply symmetry of spraying, since the spray is transported onto the vessel by the relative wind. The ship speed relative to the waves is given by (Aksyutin 1979)

$$v_{\mathrm{sw}} = 1.56 T_{\mathrm{s}} + v_{\mathrm{s}} \cos(\pi - \alpha), \tag{3.3}$$

where T_{s} is the significant wave period, v_{s} is the ship speed and α is the angle between the ship velocity vector and the wave celerity (phase velocity) vector. The wave celerity vector is taken to be parallel to the 10 m wind vector. Because (3.1) specifies no finite upper bound to the spray jet, a practical upper limit is estimated as follows. The maximum height of the spray jet is estimated from

$$H_{\mathrm{m}} = H_{\mathrm{s}} + \frac{v_{\mathrm{sw}}^2}{2g}, \tag{3.4}$$

where g is the acceleration due to gravity. The second term on the right is based on the premise that the spray jet is launched vertically with a speed equal to v_{sw}, and that air drag can be ignored. Hence it most likely overestimates the actual spray jet height. However, this is not a serious concern because of the rapid reduction of LWC with height given by (3.1).

Spray jets are not generated with every ship–wave encounter (Aksyutin 1979; Panov 1976; Horjen & Carstens 1990). Zakrzewski (1987) has observed spray jet generation with every second wave on a fishing trawler. I. Horjen (personal communication) has observed spray jet generation with every fourth wave encounter on a large whaling vessel. The latter result was adopted in the model. The wave encounter interval, P_{w}, is given by Aksyutin (1979)

$$P_{\mathrm{w}} = \frac{1.56 T_{\mathrm{s}}^2}{v_{\mathrm{sw}}}. \tag{3.5}$$

The duration of a spray event, P_{s}, is adapted from the formula proposed by Zakrzewski (1987) for a fishing trawler,

$$P_{\mathrm{s}} = \frac{10.0 v_{\mathrm{sw}} H_{\mathrm{s}}}{U^2}, \tag{3.6}$$

where U is the 10 m wind, and the constant has been adjusted for consistency with the observed spray duration on the USCGC *Midgett* of 3 to 5 s (Ryerson 1995).

(iii) *Equations of motion and thermodynamics of the spray droplets*

The model uses the Zarling (1980) formulation to compute the trajectory and thermal evolution of droplets of diameter 1.75 mm. The droplets are assumed to be spherical, and coalescence and break-up are ignored. Evaporative cooling is considered, but the effect of evaporation on droplet mass is negligible, and hence neglected. The droplet motion is confined to a vertical plane and its trajectory is calculated in a frame of reference translating with the vessel. Initially, the droplet is taken to be at rest, relative to the ship, and its subsequent motion is controlled by air drag and gravity. The trajectory is computed until the horizontal coordinate along the trajectory, ξ, exceeds the length of the ship.

The droplet equation of motion is

$$\frac{\mathrm{d}\boldsymbol{v}_\mathrm{d}}{\mathrm{d}t} = -\frac{3}{4}\frac{C_\mathrm{d}}{D}\frac{\rho_\mathrm{a}}{\rho_\mathrm{w}}|\boldsymbol{v}_\mathrm{d} - \boldsymbol{U}|(\boldsymbol{v}_\mathrm{d} - \boldsymbol{U}) - \boldsymbol{g}\left(\frac{\rho_\mathrm{a}}{\rho_\mathrm{w}} - 1\right), \tag{3.7}$$

where D is the droplet diameter, $\boldsymbol{v}_\mathrm{d}$ the droplet velocity, $\boldsymbol{U}$ the (constant) 10 m wind speed, $\boldsymbol{g}$ the acceleration due to gravity, ρ_a the air density, ρ_w the brine density and C_d the droplet drag coefficient according to Langmuir & Blodgett (1946),

$$C_\mathrm{d} = \frac{24.0}{Re} + \frac{4.73}{Re^{0.37}} + 6.24 \times 10^{-3} Re^{0.38}, \tag{3.8}$$

where Re is the droplet Reynolds number. The two scalar components of (3.7) were solved numerically using the Euler method with a time-step of 5 ms.

The initial temperature of the droplets in the spray jet is taken to be that of the sea surface. Subsequently, the droplets cool and eventually supercool due to convective, evaporative and radiative heat transfer with the airstream. We ignore any temperature gradients in the droplets, assuming them to be thermally homogeneous. Unlike other models (e.g. Stallabrass 1980), the range of the droplet trajectories is not fixed, and hence the impact temperature of the impinging spray varies over the vessel, generally decreasing with distance aft. The droplet cooling equation may be expressed as

$$mc_\mathrm{b}\frac{\mathrm{d}T_\mathrm{d}}{\mathrm{d}t} = 4\pi r^2(C + E + R), \tag{3.9}$$

where m is the droplet mass, c_b is the specific heat capacity of the brine, T_d is the droplet temperature, and r is the droplet radius. The terms C, E and R are the convective, evaporative and long-wave radiant heat fluxes, respectively. These may be expressed as follows

$$\left.\begin{aligned} C &= h_\mathrm{c}(T_\mathrm{d} - T_\mathrm{a}), \\ h_\mathrm{c} &= \frac{Nuk_\mathrm{a}}{D}, \\ Nu &= 2.0 + 0.6Pr^{0.33}Re^{0.5}, \end{aligned}\right\} \tag{3.10}$$

where h_c is the convective heat transfer coefficient of the droplet, T_a is the air temperature, k_a is the thermal conductivity of the airstream, D is the droplet diameter, Nu is the droplet Nusselt number and Pr is the Prandtl number of the airstream,

$$\left.\begin{aligned} E &= h_v \rho_a l_v (q_d - q_a), \\ h_v &= \frac{Sh D_w}{D}, \\ Sh &= 2.0 + 0.6 Sc^{0.33} Re^{0.5}, \end{aligned}\right\} \tag{3.11}$$

where h_v is the convective mass transfer coefficient for water vapour in air, q_d is the saturation specific humidity at the temperature of the droplet, q_a is the specific humidity in the airstream, ρ_a is the density of the airstream, l_v is the specific latent heat of vaporization at the droplet temperature, Sh is the droplet Sherwood number, D_w is the diffusivity of water vapour in air and Sc is the Schmidt number of the airstream.

$$R = \varepsilon \sigma (T_d^4 - T_a^4), \tag{3.12}$$

where ε is the droplet emissivity (taken here to be unity) and σ is the Stefan–Boltzmann constant.

Because the droplets are large, a spray collision efficiency of unity is assumed for all ship components. For the cells that are sprayed, the spray flux is given by

$$F_s = wA(\boldsymbol{v}_s \cdot \hat{\boldsymbol{n}}), \tag{3.13}$$

where w is the liquid water content in the spray jet at the point of origin of the trajectory, A is the area of the grid cell, $\boldsymbol{v}_s$ is the impact velocity of the spray and $\hat{\boldsymbol{n}}$ is the unit inward normal vector to the grid cell surface. The droplet impact velocity is interpolated along the computed trajectory at the point where the trajectory intersects the centre of the grid cell. Equation (3.13) is based on the steady-state conservation of mass flow along flux tubes that are bounded by droplet trajectories.

(iv) *Ice growth*

The conceptual model of water delivery and ice accretion

The icing model has a fast and slow time dependence. The slow time dependence responds to hourly changes in the environmental conditions. The fast time dependence responds to changes in liquid flux during a single spraying event, in particular the transition from spray impingement to spray-free conditions. The total duration of a spraying event is taken to be the interval between sprays, namely $4P_w$. The time-step for the icing computations during the event is 1 s. Unfrozen brine is allowed to flow downwards between grid cells after each time-step, so that, even after spraying has ceased, unfrozen brine may continue to flow and produce additional ice accretion. However, because the model considers only a single spraying event, any unfrozen brine remaining at the end of the event is ignored. In addition, because the model does not take into account lateral or longitudinal flow of brine, the transport of brine from component to component is not considered. A single spraying event can therefore be divided into three distinct intervals: first, the interval during which spray is impinging upon a grid cell, P_s, which is a constant for all grid cells; second, the interval following direct spraying during which unfrozen brine continues to flow

over the ship's surface (this varies from grid cell to grid cell); and third, if all the brine eventually freezes, the interval prior to the next potential spraying event, during which no spray impingement, brine flow or accretion occurs. The total duration of all three intervals is $4P_{\mathrm{w}}$.

The conceptual model of the icing system in each grid cell consists of an underlying steel plate, which is assumed to play no role in the process other than to provide a substrate for the ice, and an overlying accretion layer, consisting of pure ice and entrapped brine pockets. Surmounting this, there is a layer of unfrozen brine and finally the cold airstream. It is assumed that the accretion layer and the unfrozen brine are at the same spatially uniform temperature. This temperature is the equilibrium freezing temperature of the entrapped brine and the overlying unfrozen brine, which are assumed to have the same salinity.

Heat transfer and pure ice growth

Four heat fluxes control the rate of pure ice formation in each grid cell: the convective heat flux, Q_{c}; the evaporative heat flux, Q_{e}; the radiative heat flux, Q_{r}; and the sensible heat flux associated with both the directly impinging spray and the surface flow of unfrozen brine, Q_{s}. The convective heat flux is given by

$$Q_{\mathrm{c}} = h(T_{\mathrm{s}} - T_{\mathrm{a}}), \tag{3.14}$$

where T_{s} is the equilibrium freezing temperature of the surface brine, T_{a} is the air temperature and h is the local convective heat transfer coefficient. h is considered to be a constant for all of the grid cells of a particular component, but varies from component to component. It is determined from the Nusselt number for the surface, Nu,

$$h = \frac{Nuk_{\mathrm{a}}}{L}, \tag{3.15}$$

where k_{a} is the thermal conductivity of air and L is the characteristic length of the component. The Nusselt number is determined as follows

$$Nu = \begin{cases} 0.036Pr^{0.33}Re^{0.80} & \text{for planar components,} \\ 3.0Re^{0.50} & \text{for cylindrical components,} \end{cases} \tag{3.16}$$

where Pr is the Prandtl number for the airstream and Re is the Reynolds number of the component, defined using the relative wind speed and the characteristic length of the component. The characteristic dimension is taken to be the diameter for cylindrical components and the maximum dimension along the direction of the relative wind for planar components.

The evaporative heat flux is given by

$$Q_{\mathrm{e}} = \frac{\varepsilon l_{\mathrm{v}}}{pc_p}\left(\frac{Pr}{Sc}\right)^{0.63} h(e_{\mathrm{s}} - e_{\mathrm{a}}), \tag{3.17}$$

where ε is the ratio of the molecular weights of water vapour and dry air, l_{v} is the specific latent heat of vaporization at the surface temperature, p is the atmospheric pressure, c_p is the specific heat of air at constant pressure, Sc is the Schmidt number for air, $e_{\mathrm{s}} = e_{\mathrm{s}}(T_{\mathrm{s}})$ is the saturation vapour pressure over the brine surface and

$e_a = re_s(T_a)$ is the partial pressure of water vapour in the airstream, with r the relative humidity. Neglecting the effect of salinity on the saturation vapour pressure, it is calculated using the Bolton formula for fresh water,

$$e_s(T) = 611.2 \exp\left(\frac{17.67T}{T + 243.5}\right). \tag{3.18}$$

The radiative heat flux is give by

$$Q_r = 4.4(T_s - T_a), \tag{3.19}$$

which approximates linearly the black body radiative heat exchange between the icing surface and the airstream, the emissivity of both being taken to be unity.

Finally, the sensible heat flux is given by

$$Q_s = Rc_w(T_s - T_i), \tag{3.20}$$

where R is the total brine flux to the grid cell, both from impinging spray and from run-off from other cells, c_w is the specific heat capacity of the brine and T_i is the mean temperature of all the incoming brine.

It should be noted that all of these fluxes are defined in such a way that they are positive if they represent a heat loss to the system and hence can contribute to ice formation. Thus the rate of pure ice formation, I, is given by

$$I = \frac{Q_c + Q_e + Q_r + Q_s}{l_f}, \tag{3.21}$$

where l_f is the specific latent heat of freezing of pure ice at the surface temperature. Equation (3.21) cannot be solved directly because T_s is an unknown. We take this to be the equilibrium freezing temperature of the entrapped brine and the unfrozen surface brine, both of which are assumed to have the same composition. This temperature is a function of the salinity of the unfrozen brine and it may be determined from the phase equilibrium equation once the salinity is known. The latter may be computed from the condition that salt mass is conserved, and the assumption that the pure ice rejects all salt into the brine pockets, or into the liquid surface layer, as it freezes. The resulting set of equations is solved using an approach proposed by Blackmore *et al.* (1989).

(*c*) *Brine entrapment and surface flow*

Once I has been determined, the rate of unfrozen brine accumulation, B, is simply given by

$$B = R - I. \tag{3.22}$$

However, B in itself does not specify the partitioning of the unfrozen brine between the brine pockets trapped in the ice and the liquid brine on the ice surface. Makkonen (1987) and Blackmore & Lozowski (1998) have proposed theoretical means to determine this partitioning, but neither approach is entirely satisfactory, yet. Consequently, we use the empirical results of Panov (1976) and Zakrzewski (1987), which suggest that the overall salinity of the accretion, $\hat{s}$, is *ca.* 75% of the salinity of the impinging brine, s_w,

$$\hat{s} = 0.75 s_w. \tag{3.23}$$

Equation (3.23) is used as follows to estimate brine entrapment. We may formally write B as the sum of the entrapped brine mass, B_e, and the surface brine mass, B_s,

$$B = B_e + B_s. \tag{3.24}$$

The ice fraction of the accretion, f_d, is defined as

$$f_d \equiv \frac{I}{I + B_e}. \tag{3.25}$$

The freezing fraction, f_r, is defined as

$$f_r \equiv \frac{I}{I + B}. \tag{3.26}$$

The overall salinity of the accretion, $\hat{s}$, is defined as

$$\hat{s} \equiv \frac{s_b B_e}{I + B_e}, \tag{3.27}$$

where s_b is the salinity of the entrapped brine. Equations (3.25) and (3.27) may be rearranged to yield

$$f_d = 1 - \frac{\hat{s}}{s_b}. \tag{3.28}$$

Finally, by rearranging (3.25), we have

$$B_e = I\left(\frac{1}{f_d} - 1\right). \tag{3.29}$$

In the code, f_d is calculated from (3.28), using $\hat{s}$ from (3.23), and with s_b determined from T_s. The resulting iteration is performed according to Blackmore *et al.* (1989). Based on recent marine-icing wind-tunnel experiments, f_d always exceeds *ca.* 0.5. Hence this value is imposed as a lower bound. Once I and B_e have been determined, B_s can also be readily determined. All of this surface brine flux is presumed to flow downwards to the grid cell immediately below, for vertical components (e.g. bulkheads), or to the grid cell immediately aft, for horizontal components (e.g. decks).

The entire process is repeated for each 1 s icing time-step. The accretion load on each cell during each time-step is accumulated over a single spray cycle. The load during a forecasting time-step (typically 1 h) is determined by multiplying the spray cycle load by the number of spray cycles in a forecasting time-step. The accretion thickness is calculated from the load, using an accretion density that takes into account both the pure ice and the entrapped brine. Air bubble inclusions are ignored. The accretion load on each component is determined by summing over all the grid cells in the component, and the total load on the ship is determined by summing over all components. Finally, the centre of gravity of the iceload on each component and on the entire vessel is computed.

(*d*) *Results*

We present here a sensitivity analysis of the USCGC *Midgett* icing model. The total iceload accumulated on the entire ship over 24 h, under constant environmental

Table 1. *Standard conditions used in the USCGC Midgett model*

air temperature	−17.8 °C
dew point temperature	−18.3 °C
air pressure	100.9 kPa
true wind speed	20.6 m s^{-1}
true wind direction	0°
sea surface temperature	−1.7 °C
sea surface salinity	33.5‰
fetch	926 km
ship speed	12.9 m s^{-1}
ship course	0°

conditions, is plotted against each of seven model input parameters. While each of these parameters is varied one at a time, the remaining model parameters are held constant at the standard values given in table 1. The apparently strange choice of values results from the fact that the standard parameters were originally specified using non-SI units (for example, the standard air temperature is 0 °F).

The standard conditions lead to head winds and waves and to symmetrical spraying and icing. All the model input parameters may be varied. However, it is redundant to vary both ship course and true wind direction, so the former was fixed at 0°. With these standard conditions, the model was found to be quite insensitive to air pressure and dew point temperature. Consequently, air pressure variations are not considered here, and the dew point temperature is set to 0.5 °C below the air temperature.

The air-temperature sensitivity is illustrated in figure 1*a*. It is almost linear, with the load vanishing at *ca.* −1.8 °C. The model exhibits a nonlinear sensitivity to wind speed (figure 1*b*), although it is a monotonically increasing function of wind speed. This occurs because there are several modelled physical processes that depend in various ways on the wind speed–spray jet geometry and liquid water content, the longitudinal extent of spraying, the heat transfer from the spray droplets and the heat transfer from the icing surface.

The influence of true wind direction is shown in figure 1*c*. The loads are symmetrical as the wind shifts from port to starboard, since the ship geometry is also parity symmetrical. The load increases by *ca.* 5%, from 0 to *ca.* 15°, and it then drops rapidly to zero by *ca.* 120°. These trends are qualitatively consistent with those observed on board vessels by Panov (1976) and by Tabata *et al.* (1963).

The influence of sea-surface temperature on the iceloads is shown in figure 1*d*. In all of the calculated cases, the air temperature was held constant at −17.8 °C, so no account was taken of the influence of the air temperature on the sea-surface temperature or vice versa. The sea-surface temperature is taken to be the initial temperature of the spray drops, and hence it influences the impact temperature and the sensible heat of the impinging spray. Initially, there is an almost linear trend of declining iceloads with increasing sea-surface temperature. At higher temperatures, the rate of decline is reduced, with some ice accretion occurring even at a sea-surface temperature of +12.8 °C. Of course, this is an unrealistic result, but it occurs because of the low air temperature in the model, and hence, over several seconds, the spray drops can cool below their freezing point prior to impacting on the surface of the vessel.

PHILOSOPHICAL TRANSACTIONS OF THE ROYAL SOCIETY A MATHEMATICAL, PHYSICAL & ENGINEERING SCIENCES

The variation of iceload with sea-surface salinity is shown in figure 1*e*. The model exhibits a slow, linear decline in the iceload with increasing salinity, consistent with the physics of brine ice accretions. There is, however, a physically unrealistic discontinuity at exactly zero salinity (not shown). This occurs because the ice sponginess algorithms for brine and fresh water are not suitably matched to each other. Until this matter is resolved, fresh water ice accretions are simulated in the model with a salinity of 0.1‰. With this correction, the iceload is reduced by about one-third in going from fresh water to brine of 35‰.

The influence of fetch on the iceload is illustrated in figure 1*f*. In the model, the iceload increases monotonically with increasing fetch, almost doubling as the fetch increases from *ca.* 200 to 2000 km. This is caused by increasing wave height, which enhances both the extent of the spray zone and the brine flux.

The variation of iceload with ship speed is shown in figure 1*g*. The model exhibits an approximately quadratic increase in iceload with ship speed. Ship speed influences several model processes, including the geometry and liquid water content of the spray cloud, the longitudinal extent of the spray zone and the heat transfer from the wetted surface of the ship. Clearly, the reduction of vessel speed is a powerful tool, within the control of the captain, for reducing the rate of ice accretion. Because of the nonlinearity of the relation between icing rate and ship speed, this reduction in icing rate will not be completely offset by longer transit times.

4. Modelling icing of a drilling rig

(*a*) *The ICEMOD and RIGICE models*

There are two widely used detailed numerical models that simulate and predict icing on offshore drilling rigs. These are ICEMOD (Horjen & Vefsnmo 1985, 1986*a*, *b*; Brown *et al*. 1988), developed at the Norwegian Hydrodynamic Laboratories, and RIGICE (Brown *et al*. 1988), developed by the MEP Company and Compusult Ltd for the Atmospheric Environment Service of Canada. As with the USCGC *Midgett* model, both of these models are based on structural segmentation of the rig; that is, icing is simulated separately on the various cylindrical components of the structure. Each cylindrical component is in turn segmented so that the iceload may be determined as a function of height above mean sea level.

The most recent time-dependent version of ICEMOD is based on the equations for conservation of mass, heat and salt within the brine film on the icing surface. The model takes into account local changes in these properties, as well as the thickness and flow velocity of the brine film, caused by periodic spraying, wind drag and gravity. The impinging spray flux is based on empirical expressions for the mean brine collection rate at various heights, as measured on drilling platforms at sea. A particular spray drop size distribution is assumed, and drop cooling is calculated in a manner similar to that described in § 3 *b* (iii). Also, the icing calculations of ICEMOD are essentially similar to those for the USCGC *Midgett* model, described in § 3 *b* (iv). However, in the recent versions of ICEMOD and in RIGICE, the brine salinity is calculated from the equation of Makkonen (1987),

$$s_{\mathrm{b}} = \frac{s_{\mathrm{w}}}{1 - f_{\mathrm{d}} n}, \tag{4.1}$$

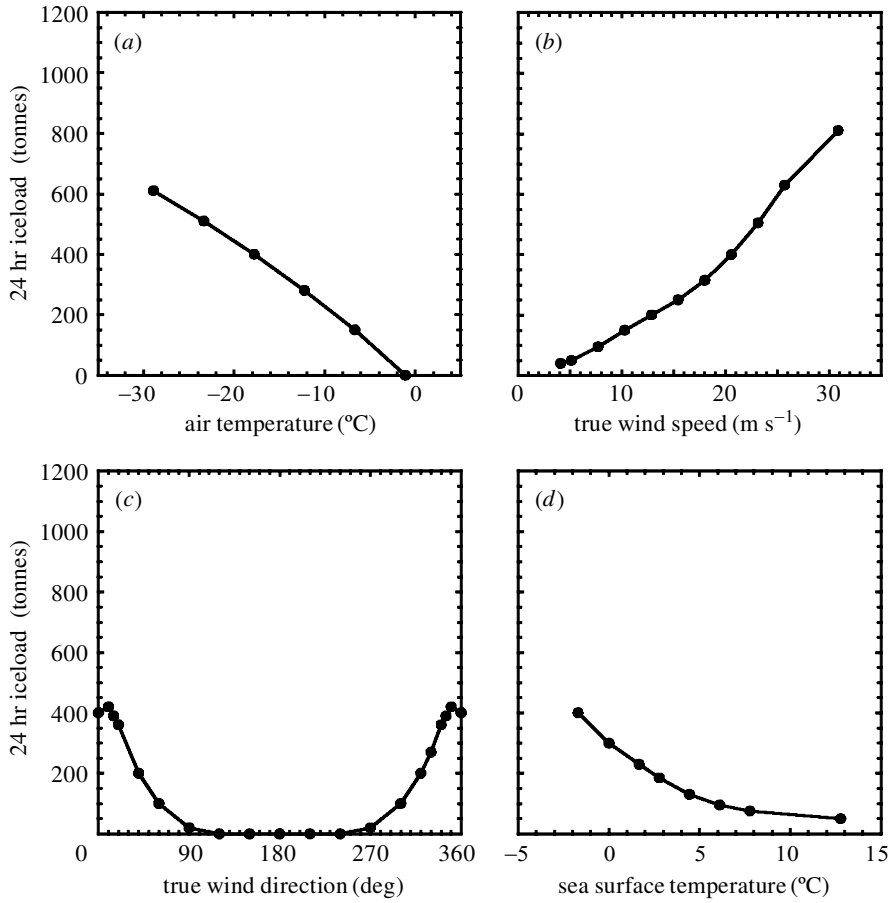

Figure 1. Influence of seven model input parameters on the 24 h iceload accumulated over the entire USCGC *Midgett*. Other model parameters are given in table 1.

with the ice fraction f_{d} taken to be 0.66 in ICEMOD and 0.72 in RIGICE. Here, n is the ratio of the rate of spongy accretion to the spray flux. Equation (4.1) retains the important feedback between the brine salinity, s_{b}, and the accretion rate (Makkonen 1987), in contrast to the procedure used in the USCGC *Midgett* icing model, described in § 3 *b*.

RIGICE is in many respects similar to ICEMOD, the principal differences being different spray flux formulations, and the fact that RIGICE operates with time mean environmental inputs, while ICEMOD is fully time dependent. RIGICE also includes some simple additional assumptions. For example, RIGICE has no drop cooling algorithm. It also assumes that any unfrozen brine is lost by wind drag, rather than flowing over the accretion surface, thereby influencing accretion on lower levels of the structure.

More details and discussion of the similarities and differences between ICEMOD and RIGICE have been given by Brown *et al*. (1988). This report also presents some model run intercomparisons and related wind-tunnel tests on cylinder icing. These results indicate that while ICEMOD behaves more realistically than RIGICE in some

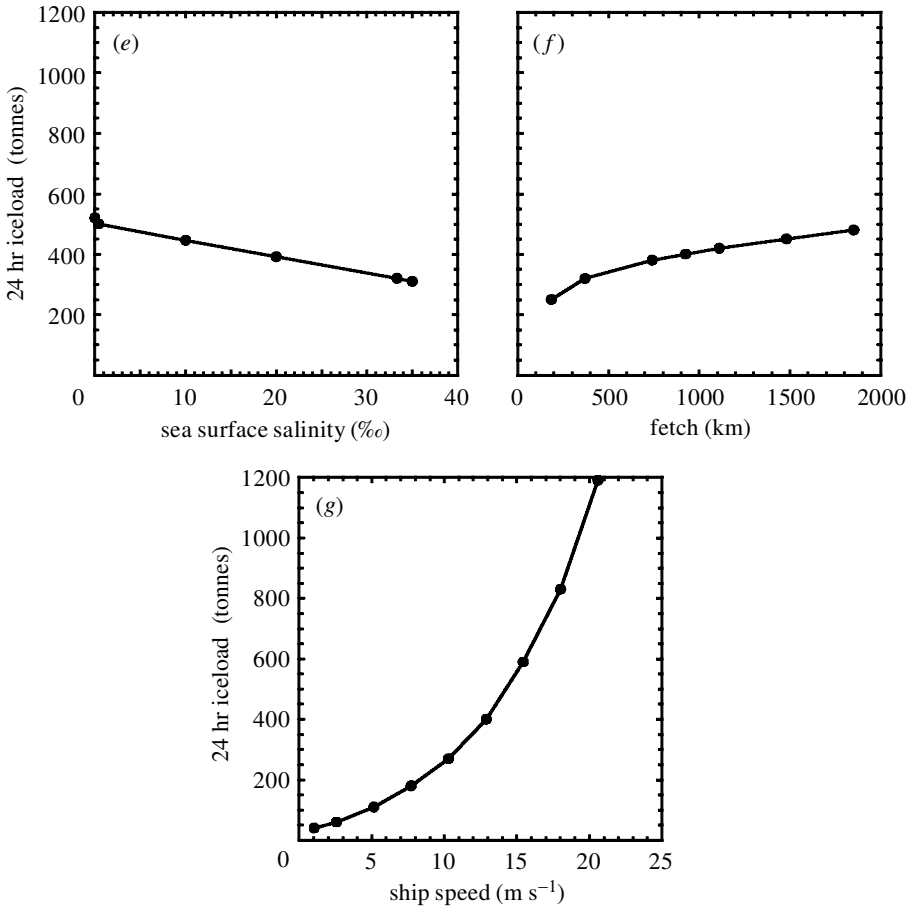

Figure 1. (*Cont.*)

individual comparisons, the correlation between the results of the two models is high, suggesting that the simplifications made in RIGICE do not necessarily weaken its overall predictive ability. It is also clear that in order to fully use such model features as drop cooling, pulsed spraying and time-dependent icing, one would need a significantly improved understanding of the processes of spray flux production, entrainment of cold air into spray clouds and the flow of unfrozen brine over accretion surfaces. Overall, unpublished comparisons of model simulations with icing data from drilling rigs have shown promising results, but inadequate data on spray flux as a function of height are a bottleneck in comparing model predictions with observations. Because of this, we present in the following sections a previously unpublished improvement to RIGICE, with simulation of wave-impact spray generation.

(*b*) *Liquid water content and spray flux*

In many marine icing models, a vertical distribution of LWC is assumed such as that given in (3.1). Based on measurements taken far from the spray source, the LWC in such formulations diminishes exponentially with height. In a vertically homogeneous wind, so does the brine flux that impacts the structure. However, when

a structure close to the ejection point of the droplets is considered, the vertical distribution of the spray flux distribution will not necessarily be exponential, since the droplets will impact in the early stages of their trajectories. In addition, the impinging brine flux distribution will depend strongly on the distance between the ejection point and the structure. Hence the vertical LWC distribution, determined from the impinging flux and wind speed, will also vary with distance from the brine droplet source.

Consequently, there is no single instantaneous or mean LWC distribution that is relevant to rig icing due to wave impact. The spray flux must instead be calculated directly using drop trajectory analysis, as, for example, was done in Chung & Lozowski (1999). The vertical brine flux distribution at any instant may be very different from the mean flux distribution. For example, the impinging brine flux distribution from a single spray event may exhibit a sharp peak at some height, rather than a monotonic decline with height. Hence the procedure used by ICEMOD, in which the spray is modelled by a pulsed occurrence of a mean water flux, is not necessarily to be preferred over the simpler stationary flux approach of RIGICE.

As discussed above, the vertical spray flux distribution averaged over many spray events may bear little similarity to the spray flux distribution during an individual spray event. Why then do observations imply a mean flux that diminishes exponentially with height? The answer is likely to be a simple one. The ejection height of spray increases with increasing wave height. In view of the distribution of wave height, one may expect that less brine will reach high levels, because there is a diminishing number of large waves. Hence it is apparent that it is only possible to simulate the spray flux onto rigs with due consideration of the wave height distribution function.

(*c*) *The new RIGICE spray model*

The new SPRAY algorithm used in RIGICE incorporates the following principal features: flux distribution calculations based solely on droplet trajectories; a dependency on wave period, wave height and wave spectrum; wave run-up on the structure; and a consideration of wave force in determining droplet ejection. The wave parameters used in the SPRAY algorithm are derived from linear wave theory, and the waves themselves are modelled as sinusoidal. The force exerted on the structure by the wave is used to determine the droplet ejection point, and the difference between the slope of a droplet's initial velocity vector and the slope of the wave at the ejection point is used as an ejection threshold condition. Currently the model ejects droplets in three dimensions, but the droplet trajectory calculations are performed in two dimensions, namely longitudinal and vertical. Hence the spray flux delivered to the structure is assumed, for now, to be laterally homogeneous.

Because wave heights in a given wave train can vary considerably, the SPRAY algorithm uses a wave height probability distribution to determine the number of waves of a particular height interval that impact the structure during a given time interval (typically 1 h). The probability density function used to represent the wave height spectrum is a Rayleigh distribution, which is valid for wave modelling over narrow-band spectra (Sarpkaya & Isaacson 1981). Currently the algorithm discretizes the spectrum into five wave height intervals, although this could be increased at the expense of additional processing time. The intervals are chosen in such a way that they centre around the mode of the distribution, for a particular significant wave

height. Each wave interval in the spectrum is characterized by its average wave height. The wave period is taken to be a constant, equal to the significant wave period. For each wave height category, the brine flux is calculated for a single spray event, then multiplied by the number of events per hour and finally averaged over the hour to obtain an equivalent continuous brine flux. The ice accretion load is calculated independently for the waves in each of the five height categories and the loads are then summed to obtain the total load for all waves.

In addition to the wave-impact flux distribution calculated in the SPRAY module, a brine flux due to wind-generated spray is also applied to the structure. This depends upon the steepness of the waves. The ice-accretion computations due to wind-generated spray flux are run concurrently with the wave-impact spray flux computations.

Within the SPRAY module, the wave is modelled as sinusoidal and the wave parameters are calculated using linear wave theory. The model inputs are the current wave height and the significant wave period. From these, the wavelength, wavenumber and celerity are calculated. Wave diffraction theory is used to calculate wave run-up on the structure and the wave position for maximum wave force on the structure, based on linearization of the phase angle results of Sarpkaya & Isaacson (1981). The initial droplet velocity components are calculated using deep water linear wave theory with the wave at the zero-force point, which occurs $\pi/2$ radians before the maximum force point. An additional vertical velocity component is added based on wave run-up, taking into account the wave force run-up rise time, t_{r}, between the zero-force and maximum-force points. A horizontal velocity component is also added based on the celerity of the wave. Droplet trajectory calculations are then performed.

The initial velocity components given to the drops are determined by

$$u = \frac{\pi H}{\tau} \mathrm{e}^{kz} \sin\theta + C, \qquad w = \frac{\pi H}{\tau} \mathrm{e}^{kz} \cos\theta + \frac{z_{\mathrm{r}} - z}{t_{\mathrm{r}}}, \tag{4.2}$$

where u, w are, respectively, the x (longitudinal) and z (vertical) components, H is the upstream height of the incident wave at zero force, τ is the significant wave period, k is the wavenumber, z is the amplitude of the incident wave at zero force, θ is the phase angle of the incident wave at zero force, C is the wave celerity, z_{r} is the wave run-up height at maximum force and t_{r} is the rise-time of the force.

Droplet trajectories are calculated one at a time from initial positions that vary in both the x and y directions, using the initial velocities given above. The difference between the absolute slope of the initial droplet velocity vector and the absolute slope of the wave at the ejection point is used as a threshold condition to determine whether or not a droplet is ejected.

A predetermined wave area is associated with droplet ejection from each wave. The number of droplets ejected is estimated as the total number of spherical droplets that would fit compactly onto a surface of this area. The droplet diameter is set by the user. The resulting brine volume is then applied to the discrete vertical interval on the structure, onto which the ejected droplets are found to impact following trajectory calculations. In this way, one obtains the vertical distribution of brine flux during 1 s intervals. The overall flux delivered to each vertical level on the structure is then obtained by averaging over the wave period. Finally, this flux is applied for a time interval determined by the number of impacting waves per hour. Once ice-

accretion calculations for the current wave height increment in the spectrum have been completed, a new wave height interval is selected and the process is repeated.

It is likely that particularly violent spray production is associated with steep waves. However, the theory elaborated above, in particular the force and ejection point computations, is applicable only to waves of small to moderate steepness. Steep waves are characterized by large heights and short periods. The upwind surface is steep while the downwind surface is less so. For such waves, the calculation of the droplet ejection point, as described above, tends to initiate droplet ejection at unrealistic distances from the structure. Hence, for very steep waves, an adjustment factor is incorporated into the model. This factor has little effect on the calculated ejection point for waves of low steepness, but it moves the ejection point *ca.* 50% closer to the structure for the steepest waves.

Experimenting with this calibrated icing model for a drilling rig has led to some promising results. However, the basic processes of spray generation and ejection on impact between a wave and a structure remain poorly understood. The algorithm used in RIGICE and described above has given some insight into this problem, but it is only a modest first attempt, as several critical factors, including spray droplet size, are inputs rather than outputs of the model.

5. Morphogenetic models

One of the features of marine ice accretions that continuous models of the sort described above are unable to capture is the complexity of the ice structure. Even time-dependent ice-accretion models (e.g. Baker *et al*. 1986; Szilder *et al*. 1987; Poots & Skelton 1990) have a limited ability to simulate the observed complexity of large ice accretions. Although we have no firm proof, we suspect that this complexity leads to a number of important physical effects, all of which may tend to increase the iceload. First the surface area of the accretion is increased. This will enhance the collection of directly impinging spray and of surface brine flows. It is also likely to increase the total heat transfer from the surface, and possibly also the average heat flux. In addition, pendant ice formations (e.g. icicles) can form from dripping brine that would otherwise be lost.

Since much of this surface complexity appears to arise from the freezing of surface brine flows, it was necessary to devise a modelling method that could take these into account, in complex geometries that evolve in response to the process that creates them. Szilder (1993, 1994) was the first to develop such techniques and to apply them to ice accretion on cables under freezing rain conditions. Subsequent development and analysis of this type of model has led to the conclusion that they are also applicable to marine icing simulation, although computer limitations have so far constrained their application to relatively small domains. In addition, sponginess and salinity effects have not yet been taken into account. Ways of relating the microscopic model parameters to the macroscopic environmental parameters are also still under development. Nevertheless, we believe that this modelling approach holds sufficient promise for application in the marine environment that we describe it here in some detail and show a number of examples of what can be done with it. We call this approach morphogenetic modelling because the shapes of ice structures that are formed are determined largely by the particle flow and freezing processes, rather than by the boundary or initial conditions of the problem. What this means is that

ice structures can develop, particularly pendant ice structures, that bear little resemblance to the surface on which they are formed. One of the consequences is that the modelled structures are 'chaotic'. That is, two slightly different initial conditions can give rise to two ice accretions that are similar in overall structure but different in detail.

The central premise of this modelling approach is not new. Its aim is to build up an ice-accretion structure using discrete elements or 'particles'. Lozowski *et al*. (1983) demonstrated how such a method could be used to simulate the growth of single rime feathers. In this case, the discrete elements were individual liquid droplets that froze as spheres on impact. Gates *et al*. (1988) extended the method to simulate rime icing on a fixed cylinder, while Personne *et al*. (1990) have used it to simulate icing on a rotating cylinder. In all three papers, the impacting particles were assumed to freeze at the point of contact with the existing ice structure. The resulting structures tend to have a low density with many air inclusions, much like natural low-density rime. In order to simulate the formation of ice with higher densities, it was necessary to allow the impacting particles to migrate along the existing accretion surface and to insinuate themselves into crevices and voids within the ice structure. By allowing limited droplet mobility after impact, Lozowski *et al*. (1991) were able to produce quite realistic simulations of the structure of giant hailstones. Szilder (1993) extended this approach to allow much greater particle mobility. The particle mobility was formulated in the model using a Monte Carlo approach, leading to a 'random walk' of the particle along the accretion surface.

The morphogenetic model, as it is described here, consists of a ballistic trajectory model that determines where the particles impact and a random walk model that controls the surface motion and freezing of the particles. While it is not absolutely necessary, it is much easier to keep track of particle motion and location if the particles move through a lattice. We use a simple rectangular lattice. Although the particles are indeed fluid 'elements', we have not found it illuminating to attempt to define a one-to-one correspondence between the particles and impacting liquid drops, or between the particles and coherent structures within the surface liquid flow. While this complicates the interpretation of the model 'physics', it does not preclude the ability to make a connection between the microscopic model parameters (the random walk probabilities) and the macroscopic environmental conditions, such as air temperature, wind speed and so on.

The details of the two- and three-dimensional versions of the model have been described fully by Szilder (1994) and by Szilder & Lozowski (1995*a*). Consequently, we will describe here only the highlights. In two dimensions, we will consider the formation of an icicle under a horizontal surface, and the accretion of ice on a horizontal cylinder with vertically falling particles. We will then examine the same configurations in three dimensions and, in addition, the accretion of ice on a hemisphere with vertically falling particles.

(*a*) *The two-dimensional model*

A two-dimensional model was created first, largely for the sake of computational efficiency. However, it has the advantage of more convenient visualization, since the particles move within a two-dimensional rectangular lattice. The icing substrate is defined by filling appropriate lattice cells. Then a particle is fired at the substrate

from a random location on one of the boundaries of the domain. Prior to impact, the trajectory is taken to be a straight line. The particle is said to strike the icing substrate (or the existing accretion) when it arrives at a lattice location with at least one occupied neighbour. Once on the surface, the particle's motion is determined by a few simple stochastic rules. At each step in the process, there are five possible future states for a particle. It may move one cell in any of four directions—left, right, up or down (diagonal motion is not allowed)—or it may freeze *in situ*. We specify a probability for each of these events. In order to minimize the number of independent model parameters, the probabilities of upward and horizontal motion (left and right) are equated. This is called the motion probability. The ratio of the probability of downward motion to the probability of motion in any other direction is called the 'motion parameter'. We conjecture that its value is related to the relative magnitude of gravity, surface tension and viscous forces. The freezing probability is the probability, at each step in the particle's random walk, that it will freeze. The freezing probability must clearly be related to the heat flux between the icing surface and the airstream. Since the sum of all five probabilities is unity, specifying the motion parameter and the freezing probability suffices to define the model. Making the link between these microscopic model parameters and the macroscopic physical and environmental conditions is the most difficult aspect of this type of modelling. As we will describe later, this is done, essentially, by performing numerical experiments.

Having specified the model probabilities, the particle's actual next move is determined using a random number generator along with a cumulative probability distribution for the particle's behaviour. The particle is, however, constrained not to move into an already occupied cell, nor to move to a cell with no occupied neighbours. The latter constraint prevents the particle from walking away from the existing ice or substrate surface.

The random walk of the particle may end in one of two ways. The first is by freezing, if a random number corresponding to the freezing probability interval is drawn. Should this happen, the particle does not necessarily freeze in its present grid cell. Instead, a 'cradle' location is sought in the immediate neighbourhood of its present location. The purpose of this procedure is to densify the resulting ice matrix. Physically, this may be thought of as accounting for the effect of surface tension in moving liquid into cracks and voids in the ice matrix, where it will subsequently freeze. A cradle location is sought within a square domain, centred on the particle's present position. The side of the square is of length $2n + 1$. We call n the 'freezing range parameter', and we typically specify values between 1 and 5. The particle that is about to be frozen is moved to the empty cell within this square, where it will have the maximum number of occupied neighbours. If there is more than one such site, the final site is chosen randomly from among them. For small values of the freezing range parameter, the ice structure remains quite porous (Szilder 1993), while for large values it tends to be dense and to adopt a smooth surface.

The particle may also cease its random walk if it is shed from the ice structure. This is allowed to occur in the model if the particle reaches a local minimum in the surface topography (for example, the tip of an icicle). If the particle remains at this level without freezing for a critical number of time-steps, referred to as the 'shedding parameter', it is allowed to drip from the structure. Once a particle's motion is terminated, either by freezing or by dripping, the next particle is released.

The procedure may in principle be continued indefinitely, but constraints of computer time and storage have so far limited typical particle numbers in two dimensions to several thousand.

(i) *Icicle formation*

Makkonen (1988*a*), Szilder & Lozowski (1994*b*) and Chung & Lozowski (1990) have all published continuous models of icicle formation. The advantage of the present method over these traditional approaches is its ability to simulate more complex pendant ice formations. Nevertheless, the simulation of single icicles is an appropriate test of the model. In order to make the problem two dimensional, cylindrical symmetry is assumed, as in the classical models. However, in order to distinguish the resulting two-dimensional model from a slab-symmetrical one, the number of particles required to completely fill a grid cell increases quadratically with radius, starting at unity along the axis. The particles are released at the icicle root and move downward along the existing ice surface. The relations used to specify the freezing probability and shedding parameter as a function of the ambient conditions have been derived by Szilder & Lozowski (1994*a*).

Figure 2 shows an example of the shape evolution of four icicles. Smooth curves have been fitted to the actual surface, which is discrete. As a result, earlier and later surfaces occasionally intersect. The resulting ribs are a consequence of the stochastic nature of the model, although they do tend to exhibit some temporal continuity. The fact that their length-scale is comparable with that observed in icicle ribs may simply be a coincidence, however. In order to illustrate the stochastic nature of the model, two simulations with identical model parameters, but using different random number sequences, have been juxtaposed in figure 2*e*, the right-hand side being identical to figure 2*d*. Interestingly, this produces a more realistic 'effect', although it is not physically meaningful in the context of a cylindrically symmetric model. Figure 2 shows that for these cases, icicle mass and cross-section both increase with increasing heat flux. The icicle length, however, may increase or decrease with increasing heat flux. The water supply rate does not appear to influence the mean cross-sectional area of the icicles, while the icicle mass and length may either increase or decrease as the supply rate rises. Szilder & Lozowski (1994*a*) have shown that the final icicle length, diameter and mass, as a function of the external heat flux and liquid supply rate, agree well with both experimental data and classical continuous icicle models.

(ii) *Ice accretion on a cylinder*

Here we examine a slab-symmetrical model of ice accretion on a horizontal cylinder under vertically impinging freezing spray conditions in calm winds. By analogy with the freezing rain problem, the spray flux is specified in mm h^{-1}. Details of the model and the derivation of relations relating model parameters to ambient conditions have been given by Szilder (1994). In the model, the particles are fired at the cylinder along straight vertical trajectories from a random position along the upper boundary of the domain. The particle's subsequent random walk is identical to that described above in connection with the icicle model.

The influence of the mean convective heat flux on the total impinging spray mass and the distribution of the ice mass is shown in figure 3*a*. The total impinging spray

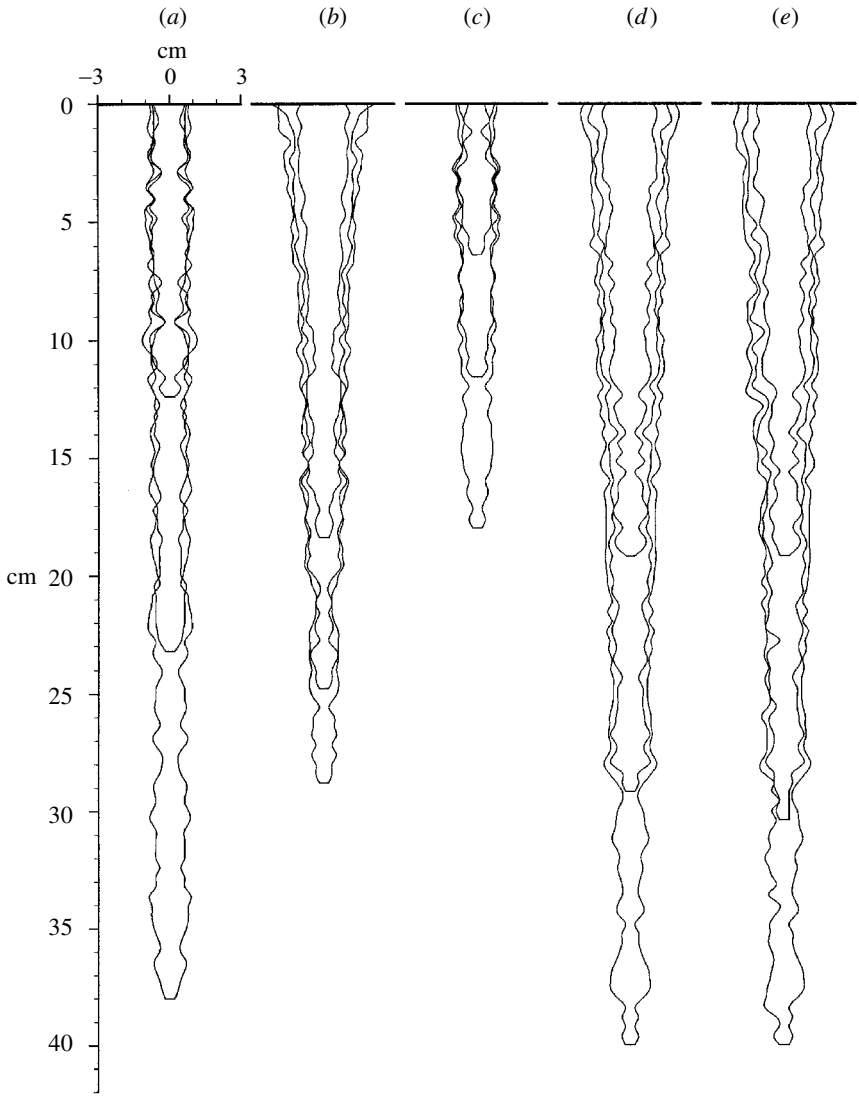

Figure 2. Evolution of the icicle shape with time. The total time of the simulation is 120 min and shapes are displayed every 40 min. The following values of the liquid supply rate and heat flux from the icicle surface have been assumed: (*a*) 15 mg s^{-1} and 40 W m^{-2}; (*b*) 15 mg s^{-1} and 400 W m^{-2}; (*c*) 30 mg s^{-1} and 40 W m^{-2}; (*d*) 30 mg s^{-1} and 400 W m^{-2}; (*e*) the same as (*d*), but profiles from two different simulations are juxtaposed.

mass increases slowly with increasing heat flux, because the horizontal cross-section of the accretion increases with the heat flux. As a result, more spray is intercepted over the duration of the numerical experiment. As the heat flux rises, the total accretion mass increases rapidly at first, and then more slowly, until it equals the impinging spray mass at a heat flux of *ca.* 100 W m^{-2}. The uniform ice layer mass is defined to be twice the ice mass accreted on the upper half of the cylinder. This is intended to represent the portion of the ice mass that is not in the form of icicles.

In order to do this, we imagine the lower half of the cylinder to have an ice accretion that is the mirror image of the accretion on the upper half of the cylinder. The uniform ice layer mass increases essentially linearly with heat flux. Because of the way in which it is defined, it can exceed the total impinging spray mass, when most of the ice accretes above the centreline of the cylinder, but we truncate the graph of uniform ice layer mass at that point. The difference between the two mass curves is a measure of the pendant ice (icicle) mass, which increases initially with heat flux, achieving a maximum at *ca.* 100 W m^{-2}, and then subsequently decreases as the heat flux rises still further.

Various linear measures of the geometry of the accretion are shown in figure 3*b*. These are: the thickness of the uniform ice layer; the vertical coordinate of the accretion's centre of mass, measured upwards from the centre of the cylinder; and the pendant accretion length, defined as the distance between the bottom of the cylinder and the lowest part of the accretion (plotted as a negative quantity). At low values of the convective heat flux, ice forms only on the lower part of the cylinder. As the heat flux increases, some ice begins to form on the upper part of the cylinder and the centre of mass rises. It then falls again as an icicle begins to form, achieving a minimum at *ca.* 50 W m^{-2}. Still higher heat fluxes cause more ice to form on the cylinder, leading to upward motion of the centre of mass, which rises above the cylinder axis at a heat flux of *ca.* 170 W m^{-2}. The accretion length exhibits a similar behaviour, consistent with the variations of the centre of mass. However, the uniform ice layer thickness simply increases linearly with increasing heat flux. The resulting variations in accretion shape are shown in figure 4, where it can be seen that icicle formation is a strong function of the convective heat flux.

Figure 5*a*,*b* shows the influence of spray flux on the accretion mass and geometry, assuming a constant value for the convective heat flux of 30 W m^{-2}. At a spray flux below *ca.* 1 mm h^{-1}, the sensible heat flux of the warm spray is small relative to the convective heat flux, with the result that most of the impinging liquid freezes on the upper half of the cylinder and there is no dripping. When the spray flux reaches 1 mm h^{-1}, there is sufficient liquid to cover the entire cylinder. Further increases in spray flux do not substantially alter the accretion on the upper half of the cylinder, with the result that the mass and thickness of the uniform ice layer are approximately independent of spray flux. However, with increasing spray flux, the accretion below the cylinder grows, the centre of mass moves downward (figure 5*b*) and some drops begin to fall from the tip of the ice accretion. The accretion length reaches a maximum at a spray flux of 3 mm h^{-1}. This maximum results from the influence of two competing processes. As the spray flux increases initially, the accretion length increases because there is more liquid available to form the icicle. However, at very high spray fluxes, the effect of the sensible heat of the spray reduces the net heat transfer, leading to more dripping and shorter icicles. The centre of mass also begins to rise.

A comparison between the morphogenetic model prediction for the uniform ice layer and a classical continuous model prediction is encouraging (Szilder 1994). Moreover, the icicle behaviour predicted by the morphogenetic model is in qualitative agreement with that predicted by the classical icicle growth model of Makkonen (1988*a*, *b*) and with the experimental results of Maeno & Takahashi (1984), both of which show that after an icicle reaches a certain length, further increases in the liquid supply rate will make it shorter, rather than longer.

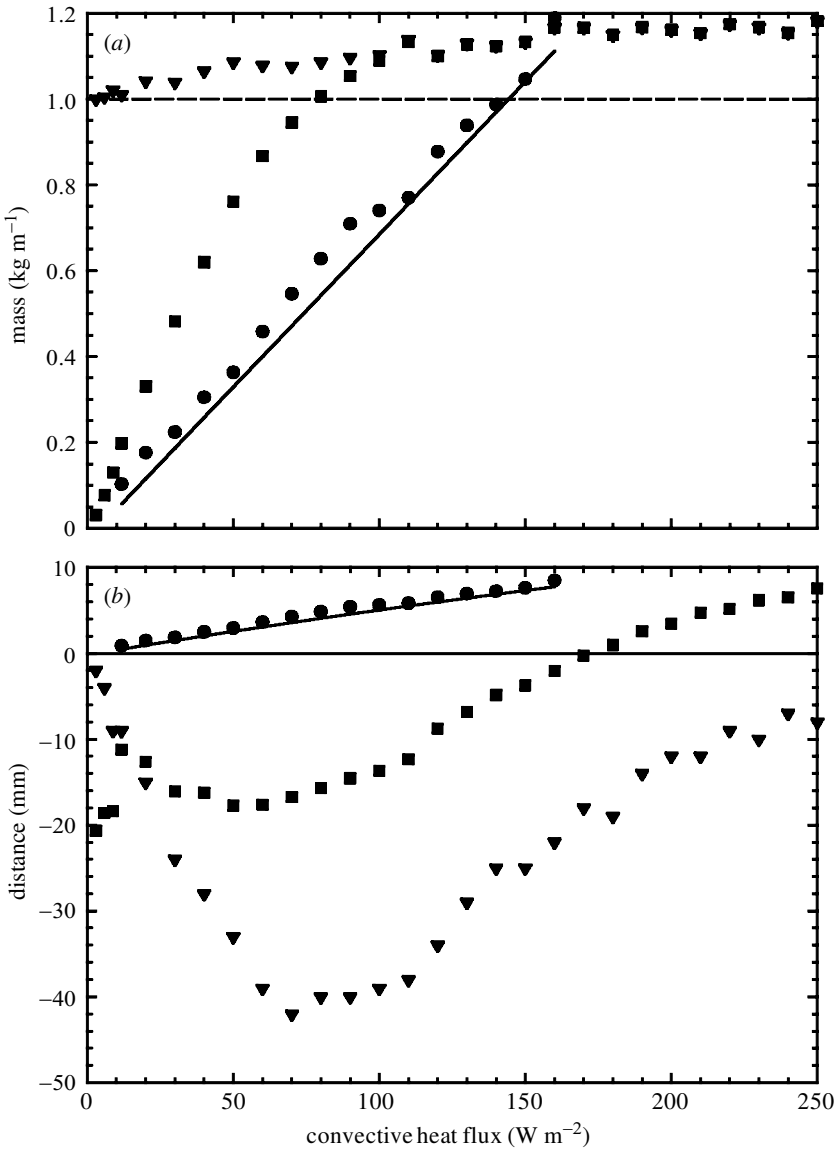

Figure 3. The influence of the convective heat flux on the accretion process. The following values have been assumed: spray flux 5 mm h^{-1}; drop temperature 2 °C; cylinder radius 2 cm; and simulation time 5 h. (*a*) Variation of the three characteristic masses. The solid line represents the uniform ice layer mass predicted by a simple energy balance model. The dashed line shows the total mass of impinging drops if the horizontal cross-section of the structure had not changed. ▼, total impinging spray mass; ■, total accretion mass; ●, uniform ice layer mass. (*b*) Changes of the three characteristic lengths. The solid line represents a prediction of the uniform ice layer thickness by a simple energy balance model. ●, uniform ice layer thickness; ■, centre of mass; ▼, accretion length.

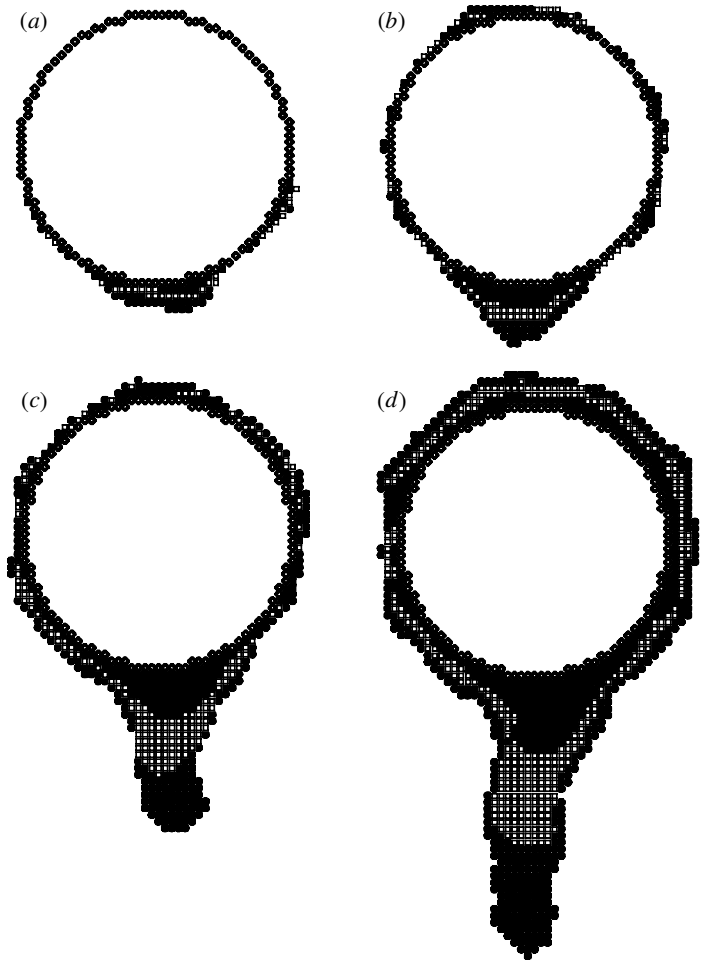

Figure 4. The influence of the convective heat flux on the shape of the ice accretion. Consecutive ice layers formed during 100 min time intervals are distinguished. The diamond shapes (◇) represent the cylinder surface. The values of the parameters are the same as in figure 3 and only the convective heat flux varies: (*a*) 5.85 W m^{-2}; (*b*) 11.7 W m^{-2}; (*c*) 30.0 W m^{-2}; (*d*) 70.0 W m^{-2}. ■, 0–100 min; □, 100–200 min; ●, 200–300 min.

(*b*) *The three-dimensional model*

The three-dimensional model is similar in principle to the two-dimensional model. The chief difference is that the random walk of the particle occurs in a three-dimensional lattice. Hence, at each step of the walk, there are seven outcomes—the particle may move one cell in any of six perpendicular directions, or it may freeze *in situ*. The ratio of the probability of downward motion to the probability of horizontal or upward motion (all of which are considered to be equal) is once again called the 'motion parameter'. Based on the numerical experiments of Szilder & Lozowski (1995*c*), it is taken to have a value of 3. As in the two-dimensional model, if the particle freezes, a suitable cradle location is sought, but this time in three dimensions. As in the two-dimensional model, the four microscopic model parameters are

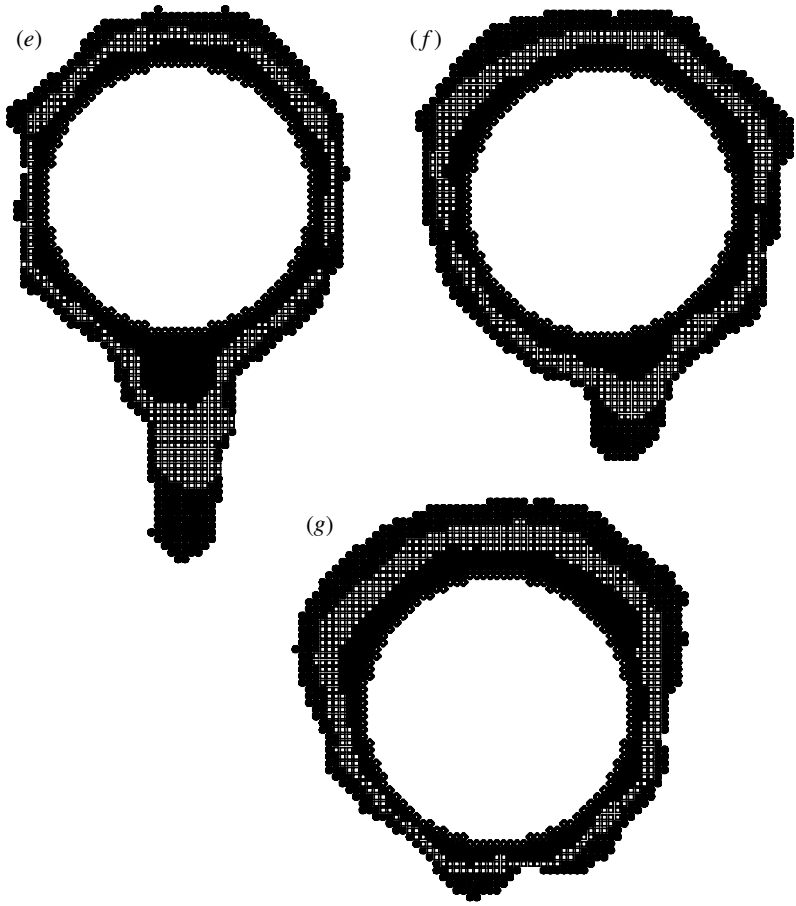

Figure 4. (*Cont.*) (*e*) 120.0 W m^{-2}; (*f*) 170.0 W m^{-2}; (*g*) 250.0 W m^{-2}. ■, 0–100 min; □, 100–200 min; ●, 200–300 min.

the freezing probability, the freezing range parameter, the shedding parameter and the motion parameter.

(i) *Icicle formation*

Szilder & Lozowski (1995*b*) have discussed the details of the three-dimensional icicle model, and have derived relations for the freezing probability and shedding parameter as functions of the ambient macroscopic conditions.

Figure 6 shows how the icicle geometry varies with air temperature. In order to aid the visualization, the shading of the particles changes after each of three consecutive 3 min time intervals. Because most of the particles freeze near the tip of the icicle, rather than along the walls, the icicle shape remains rather more cylindrical than in the two-dimensional model (contrast figure 2). Figure 7 shows the influence of air temperature on the length growth rate for two values of the supply rate, 10 and 20 mg s^{-1}. The solid curves are polynomial fits to the model predictions, which, because of the stochastic nature of the model, exhibit a 'natural' random variability. In this instance, the length growth rate increases with diminishing air temperature.

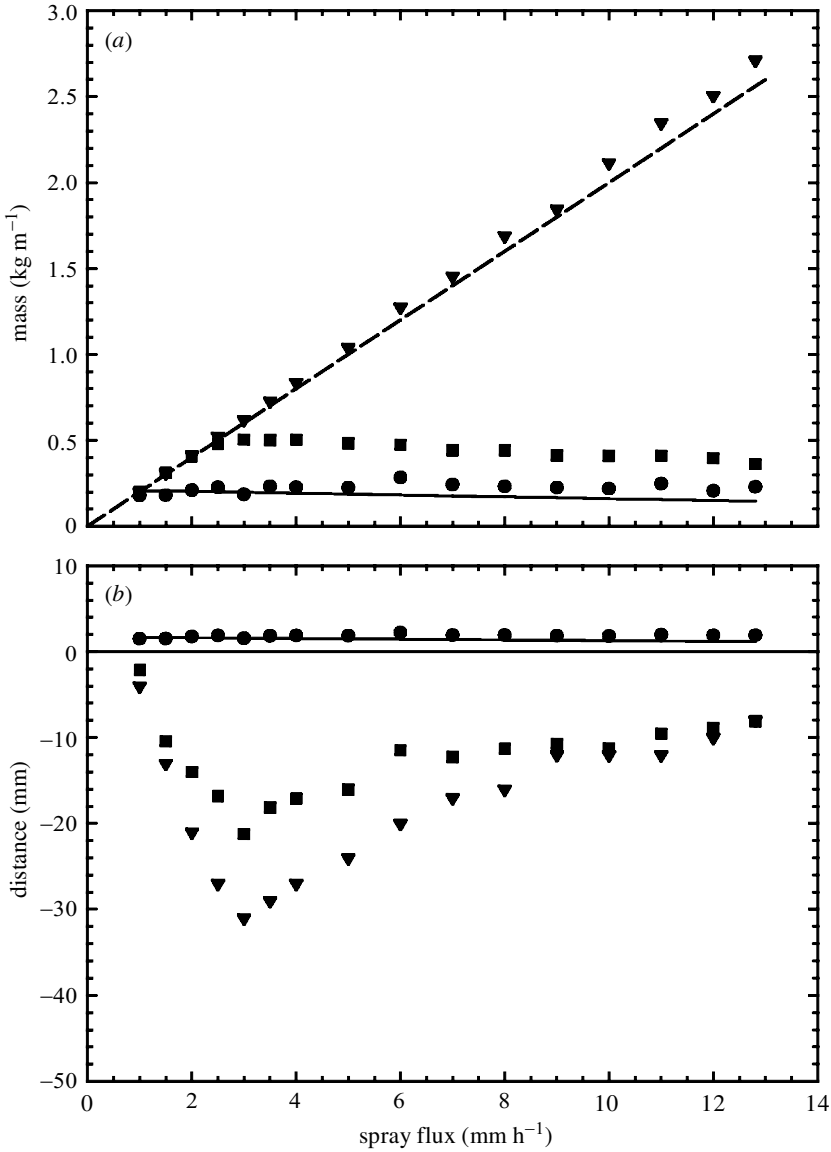

Figure 5. The influence of the spray flux on the accretion process. The following values have been assumed: convective heat flux 30 W m^{-2}; drop temperature 2 °C; cylinder radius 2 cm; and simulation time 5 h. (*a*) and (*b*) as for figure 3*a* and 3*b*.

Paradoxically, it also increases with diminishing supply rate. In order to help explain the paradox, figure 8 compares the model predictions with some experimental data, as a function of supply rate. At low supply rates there is a rapid increase in the length growth rate with increasing supply rate. The length growth rate peaks at a critical supply rate that increases with diminishing temperature. Beyond the critical supply rate, the length growth rate declines with increasing supply rate. The limited experimental data are in generally good agreement with the model, although they are

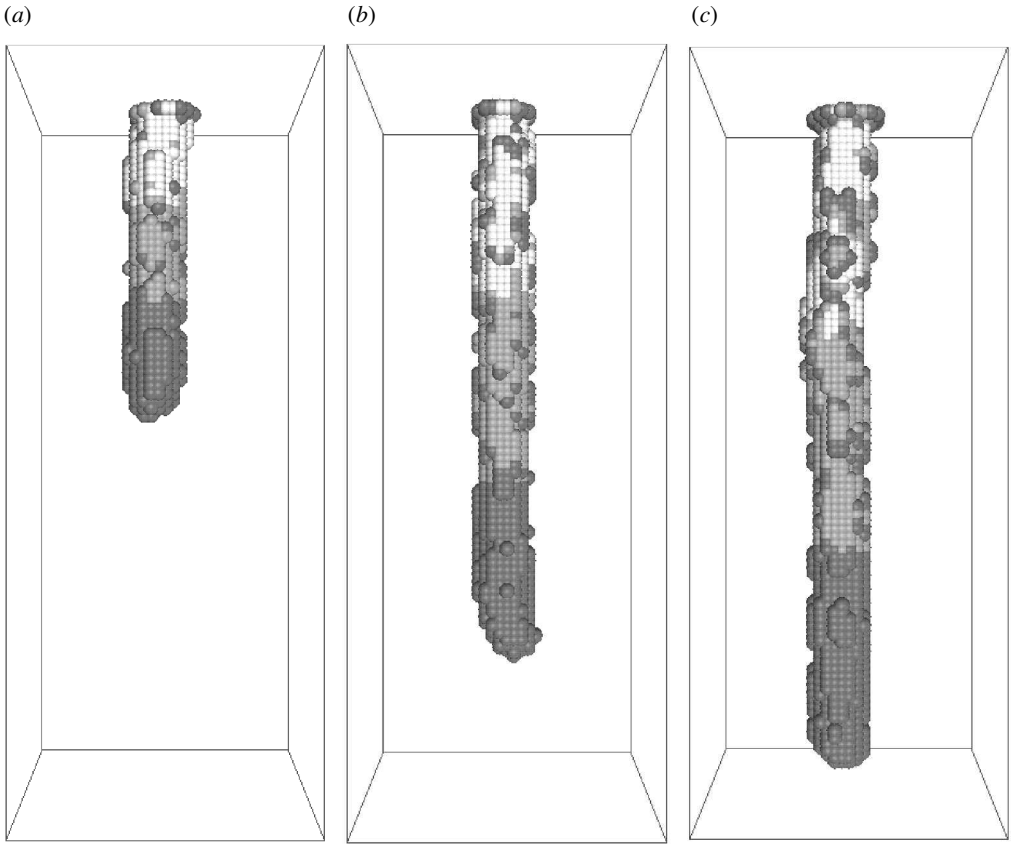

Figure 6. Evolution of the icicle shape with time for a wind speed of 3 m s^{-1} and a supply rate of 10 mg s^{-1}. The total time of the simulation is 9 min and different shading is used to distinguish three consecutive 3 min intervals. The box is 10 cm high and 4 cm wide. Air temperature: (*a*) −5 °C; (*b*) −10 °C; (*c*) −15 °C.

restricted to low values of the supply rate and hence do not confirm the existence of a peak in the growth rate curves. There is, however, quantitative agreement between our model predictions and those of Makkonen's (1988*a*) continuous model. Another prediction of the morphogenetic model that has not been confirmed experimentally is the limiting constant length growth rate of *ca.* 7 cm h^{-1} at very high supply rates.

(ii) *Complex three-dimensional ice accretions*

The power of morphogenetic modelling is its ability to simulate complex three-dimensional accretion structures, simulations that would be difficult or impossible to perform with classical continuous models. Szilder & Lozowski (1995*a*) have described the details of how the model can be applied to accretion on a non-rotating cylinder and on a hemisphere, under freezing spray conditions with no wind. These simulations were performed as functions of the microscopic model parameters, rather than the macroscopic ambient conditions. Figure 9*a* shows a three-dimensional view of the simulated ice accretion on a hemisphere, following 4 mm of freezing spray,

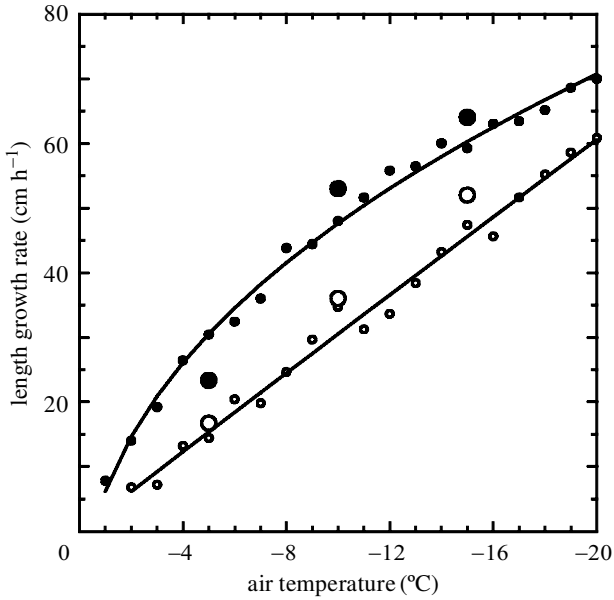

Figure 7. Length growth rate as a function of air temperature under forced convection for two values of the supply rate, 10 and 20 mg s^{-1} and wind speed 3 m s^{-1}. The experimental data are represented by large circles and the model predictions by small circles. The two solid curves are polynomial fits to the model predictions. •, 10 mg s^{-1}; ○, 20 mg s^{-1}.

with a freezing probability of 0.05% and a shedding parameter of 2000. In this case, approximately 89% of the impinging liquid mass freezes on the structure while the remainder drips off. Three well-pronounced icicles develop. If the simulation is continued with an additional 4 mm of spray, three new icicles develop and the existing icicles thicken somewhat. With additional spraying time, the length of the icicles also increases, but their number does not. The apparent discrepancy between the freezing probability (0.05%) and the freezing fraction (89%) may require some clarification. The freezing probability is the probability of freezing for a particle at each time-step. A typical particle's history involves hundreds or thousands of time-steps, hence greatly increasing the probability that it will freeze somewhere on the ice structure.

In order to ascertain what determines the number of icicles produced, the simulation was repeated a large number of times, choosing different initial seeds for the random number generator. The model parameters remained fixed for each run, and the distribution of the icicle spacing angle was examined, following 8 mm of spray. The angle was found to vary from 34 to 99°, with a median value of 56.5°. At the latter angle, the median distance between the modelled icicles is *ca.* 20 mm, a value that agrees well with experimental and theoretical results for icicle spacing (Makkonen & Fujii 1993; de Bruyn 1997). The model results also suggest that, to a first approximation, the distribution of icicle lengths is uniform. This means that there is no preferred icicle length, within the range determined by the model parameters and the ambient conditions.

Figure 9*b* is a visualization of the three-dimensional accretion on a horizontal cylinder under conditions similar to those described for the hemisphere. Once again, the predicted average icicle spacing is *ca.* 20 mm. Here too, the distribution of icicle

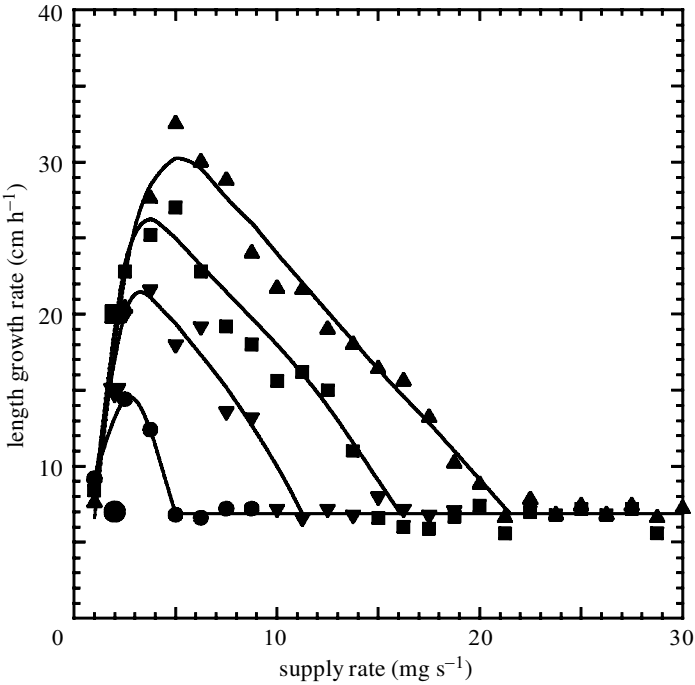

Figure 8. The length growth rate as a function of supply rate for free convection at four values of the air temperature: ●, −5 °C; ▼, −10 °C; ■, −15 °C; and ▲, −20 °C. The experimental data are represented by the large symbols and the model predictions by the small symbols. Solid lines are fits to the model predictions.

length is also approximately uniform. About 88% of the impinging water forms the ice accretion, while the rest drips. Szilder & Lozowski (1995*a*) have determined that there is an optimum value of the freezing probability (related to the heat flux from the accretion) for which icicles of maximum length form. Depending on the magnitude of the shedding parameter (related to the spray flux), the model predicts either a series of narrow finger-like icicles or thick curtain-like pendant accretions.

6. Conclusions

Over the past three decades, there has been a progression of computer model development in marine icing. The sequence that began with simple algorithms based on air temperature and wind speed has now progressed to sophisticated three-dimensional time-dependent models, and promises to incorporate morphogenetic modelling methods in the future. Meanwhile, the power of personal computers has increased so rapidly that all of these existing models can readily be run on a PC. One must be careful, however, not to confuse complexity with understanding and usefulness. Many of the processes that are modelled in three-dimensional ship-icing models are still not well understood, so that many of the equations and algorithms that are employed remain 'best estimates'. For example, we still need to improve our understanding of the time variability of spraying (spray to spray), surface brine flow, spray cloud geometry and physics, sponginess and roughness effects, heat transfer from ship surfaces and surface flow of unfrozen brine. While morphogenetic modelling is a promising

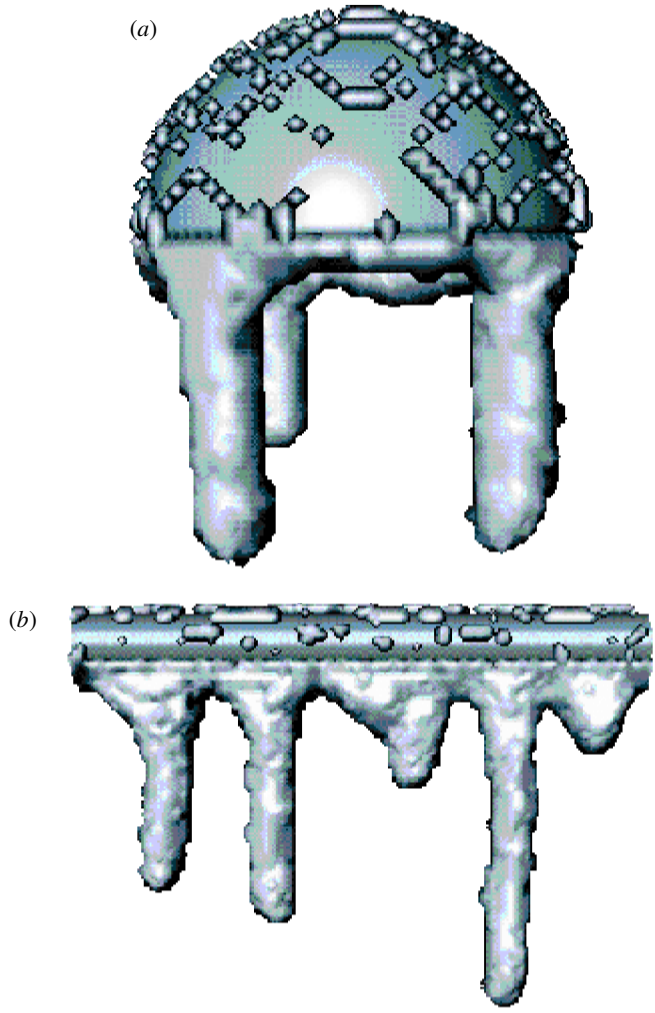

Figure 9. Ice accretion on a hollow hemisphere and a cylinder as a result of freezing spray. (*a*) Total spray equivalent depth is 4 mm; freezing probability 0.05%; shedding parameter 2000; inner and outer hemisphere radii 15 mm and 20 mm, respectively. (*b*) Total spray equivalent depth is 12 mm; freezing probability 0.05%; shedding parameter 2000; cylinder diameter 10 mm; cylinder length 100 mm.

approach for application to marine icing, there remain questions about how best to establish the relationships between the microscopic model parameters (the freezing probability, etc.) and the macroscopic environmental parameters (air temperature, etc.). Although computer power continues to increase, it is nevertheless unrealistic to expect that, in the near future, icing on an entire vessel will be simulated using a morphogenetic model. Consequently, there is still a case to be made for using simple computer models (for example, a cylinder-icing model) and linking that model output to the desired final output (iceload, for example) using experimental correlations. Full-scale field experiments are dangerous and expensive, however, so the marine-icing modeller must make judicious use of wind-tunnel measurements and

PHILOSOPHICAL TRANSACTIONS OF THE ROYAL SOCIETY A MATHEMATICAL, PHYSICAL & ENGINEERING SCIENCES

instrumental field measurements (e.g. Chung *et al*. 1988) in order to verify and calibrate whichever model is chosen for a particular application. '*Caveat emptor*' remains very prudent advice for anyone intending to use any of the models mentioned here.

The authors gratefully acknowledge the financial support of the Natural Sciences and Engineering Research Council of Canada in the production of this paper. We are also happy to acknowledge funding by the US Navy and the US Army Cold Regions Research and Engineering Laboratory for the development of the USCGC *Midgett* icing model. The authors thankfully acknowledge the contributions made by Dr C. Ryerson, Dr W. P. Zakrzewski, Dr M. Bourassa, Dr R. Z. Blackmore, Dr A. Kobos, Mr W. L. Thomas, Lt Cdr F. Lapiana, Lt Cdr P. Longo and Lt Cdr T. Terry in the development of that model. The programming of the previously unpublished parts of the enhanced RIGICE model was performed by Compusult Ltd (Mr Paul Mitten, project manager). We thank Mr Ross Brown of Environment Canada for permission to include a discussion of RIGICE in this paper. Finally, we thank Dr C. Ryerson for helpful comments on the manuscript.

References

Aksyutin, L. R. 1979 *Icing of ships*. Leningrad: Sudostroenye. (In Russian.)

Ashcroft, J. 1985 Potential ice and snow accretion on North Sea rigs and platforms. Marine Technical Note no. 1, British Meteorological Office, Bracknell.

Baker, P. C., Poots, G. & Rogers, G. G. 1986 Ice accretion on cables of various cross-sections. *IMA J. Appl. Math.* **36**, 11–28.

Bialek, E. L. 1996 *Handbook of oceanographic tables*. Washington, DC: US Naval Oceanographic Office.

Blackmore, R. Z. & Lozowski, E. P. 1994 An heuristic freezing-spray model of vessel icing. *Int. J. Offshore Polar Engng* **4**, 119–126.

Blackmore, R. Z. & Lozowski, E. P. 1998 A theoretical spongy spray icing model with surficial structure. *Atmos. Res.* **49**, 267–288.

Blackmore, R. Z., Zakrzewski, W. P. & Lozowski, E. P. 1989 Growth of ice on a ship's mast. In *Proc. 10th Int. POAC Conf., Lulea, Sweden*, vol. 3, pp. 1440–1453.

Borisenkov, Ye. P. 1969 Physical investigations of hydrometeorological complexes favourable for ship icing. In *Hyrometeorological conditions of ship icing*, pp. 7–20. Leningrad: Arctic and Antarctic Research Institute. (In Russian.)

Brown, R. D., Horjen, I., Jorgensen, T. & Roebber, P. 1988 Evaluation of state-of-the-art drilling platform ice accretion models. In *Proc. 4th Int. Workshop on Atmospheric Icing of Structures, Paris*, pp. 208–213.

Chung, K. K. & Lozowski, E. P. 1990 On the growth of marine icicles. *Atmosphere Ocean* **28**, 393–408.

Chung, K. K. & Lozowski, E. P. 1996 Offshore drilling platform icing: a review. Final Report to National Energy Board of Canada.

Chung, K. K. & Lozowski, E. P. 1999 A three-dimensional time-dependent icing model for a stern trawler. *J. Ship Res.* **42**, 266–273.

Chung, K. K., Lozowski, E. P., Pawlowski, J. S. & Xu, Q. 1995 Ship icing and stability. In *Proc. 1st Asian Computational Fluid Dynamics Conf., Hong Kong*, vol. 1, pp. 275–280.

Chung, K. K., Forest, T. W., Lozowski, E. P., Gagnon, R., Faulkner, B. & Chekhar, M. 1998 Application of new measurement and simulation methods to marine icing on offshore structures. In *Proc. 8th Int. Offshore and Polar Engineering Conf., Montreal*, vol. 2, pp. 551–558.

de Bruyn, J. R. 1997 On the formation of periodic arrays of icicles. *Cold Regions Sci. Technol.* **25**, 225–229.

Gates, E. M., Liu, A. & Lozowski, E. P. 1988 A stochastic model of atmospheric rime icing. *J. Glaciology* **34**, 26–30.

Godard, R. 1977 Numerical prediction of sea spray ice accretion on ships. Report to Atmospheric Environment Service of Canada, no. 01SZ. KM601–7-0022, part I.

Horjen, I. 1990 Numerical modelling of time-dependent marine icing, anti-icing and de-icing. Doctoral thesis, Trondheim University.

Horjen, I. & Carstens, T. 1990 Numerical modelling of the sea spray icing on vessels. In *Proc. 10th Int. POAC Conf., Lulea, Sweden*, vol. 3, pp. 694–704.

Horjen, I. & Vefsnmo, S. 1985 A numerical sea spray icing model including the effect of a moving water film. In *Proc. Int. Workshop on Offshore Winds and Icing, Halifax* (ed. T. A. Agnew & V. R. Swail), pp. 152–164.

Horjen, I. & Vefsnmo, S. 1986*a* Computer modelling of sea spray icing on marine structures. In *Proc. Symp. on Automation for Safety in Shipping and Offshore Operations, Trondheim* (ed. G. Kuo and others), pp 315–323. Elsevier.

Horjen, I. & Vefsnmo, S. 1986*b* Calibration of ICEMOD—extension to a time-dependent model. Norwegian Hydrodynamic Laboratories Report STF60 F86040.

Horjen, I. & Vefsnmo, S. 1987 Time-dependent sea spray icing on ships and drilling rigs—a theoretical analysis. Norwegian Hydrodynamic Laboratories Report STF60 F87130.

Horjen, I., Vefsnmo, S. & Bjerke, P. L. 1988 Sea spray icing on rigs and supply vessels. ESARC Report no. 15, Norwegian Hydrodynamic Laboratories Report STF60 F88137.

Jessup, R. G. 1985 Forecast techniques for ice accretion on different types of marine structures, including ships, platforms and coastal facilities. World Meteorological Organization, Marine Meteorology and Related Oceanographic Activities Report no. 15, WMO/TD-no. 70.

Kachurin, L. G. 1962 *On airplane icing theory.* Izvestiya AN SSSR, Geophysics Series, vol. 6, pp. 823–832. (In Russian).

Kachurin, L. G. & Gashin, L. I. 1969 Calculations of ice accretion on objects in a stream of supercooled aerosol with regard to icing on ships. In *Hydrometeorological conditions of ship icing*, pp. 21–32. Leningrad: Arctic and Antarctic Research Institute. (In Russian.)

Kachurin, L. G. & Morachevskii, V. G. 1965 *Kinetics of phase transitions of water in the atmosphere.* Leningrad: Leningrad State University. (Translated by Z. Lerman, Israel Program for Scientific Translations Ltd, IPST Catalogue no. 1807, 1966.)

Kachurin, L. G., Gashin, L. I. & Smirnov, I. A. 1971 Numerical estimates of the icing rate on medium tonnage fishing trawlers and seiners. *Tekhnologiya Sudostroeniya (Shipbuilding Technol.)* **6**, 113–115.

Kachurin, L. G., Gashin, L. I. & Smirnov, I. A. 1974 Icing rate of small displacement fishing vessels. *Meteoroligiya i Gidrologiya* **3**, 50–60.

Langmuir, I. & Blodgett, K. 1946 A mathematical investigation of water droplet trajectories. In *Collected works of Irving Langmuir*, vol. 10, pp. 348–393. New York: Pergamon.

Lozowski, E. P. 1988 Marine icing. In *Proc. 9th Int. Association for Hydraulic Research Symposium on Ice, Sapporo*, vol. 1, pp. 43–66.

Lozowski, E. P. & Gates, E. M. 1991 On the modelling of ice accretion. In *Freezing and melting heat transfer in engineering* (ed. K. C. Cheng & N. Seki), pp. 615–660. New York: Hemisphere.

Lozowski, E. P. & Makkonen, L. 2001 Marine icing 2001. WMO Report. (In the press.)

Lozowski, E. P. & Zakrzewski, W. P. 1993 Topside ship icing system. Final Report to the US Army Cold Regions Research and Engineering Laboratory.

Lozowski, E. P., Stallabrass, J. R. & Hearty, P. F. 1983 The icing of an unheated, non-rotating cylinder. Part I: a simulation model. *J. Climate Appl. Meteorology* **22**, 2053–2062.

Lozowski, E. P., Brett, M., Tait, N. & Smy, T. 1991 Simulating giant hailstone structure with a ballistic aggregation model. *Q. Jl R. Met. Soc.* **117**, 427–431.

Lozowski, E. P., Kobos, A. M. & Kachurin, L. G. 1996 Influence of the surface liquid film on cylinder icing under marine conditions. *J. Offshore Mechanics Arctic Engng* **118**, 158–164.

Maeno, N. & Takahashi, T. 1984 Studies of icicles. I. General aspects of the structure and growth of an icicle. *Low Temperature Sci.* A **43**, 125–138. (In Japanese.)

Makkonen, L. 1984 Atmospheric icing of sea structures. US Army Cold Regions Research and Engineering Laboratory, CRREL Monograph 84–2.

Makkonen, L. 1985 Heat transfer and icing rate of a rough cylinder. *Cold Regions Sci. Technol.* **10**, 105–116.

Makkonen, L. 1987 Salinity and growth rate of ice formed by sea spray. *Cold Regions Sci. Technol.* **14**, 163–171.

Makkonen, L. 1988*a* A model of icicle growth. *J. Glaciology* **34**, 64–70.

Makkonen, L. 1988*b* Formation of spray ice on offshore structures. *Proc. 9th Int. Association for Hydraulic Research Symposium on Ice, Sapporo*, vol. 2, 708–739.

Makkonen, L. & Fujii, Y. 1993 Spacing of icicles. *Cold Regions Sci. Technol.* **21**, 317–322.

Mertins, H. O. 1968 Icing on fishing vessels due to spray. *Marine Observer* **38**, 128–130.

MIL Systems 1993 The prevention/removal of ice accretion aboard naval surface ships: a survey of available methods. Unclassified Report to the Department of National Defence, Canada, MSEI Report 1571–26-1.

Mitten, P. 1994 Measurement and modelling of spray icing on offshore structures. Final Report to Atmospheric Environment Service of Canada, Contract no. 07SE. KM169–8-7439.

Panov, V. V. 1976 *Icing of ships*, Trudy no. 336. Leningrad: Arctic and Antarctic Research Institute. (In Russian.)

Panov, V. V. 1978 Icing of ships. *Polar Geography* **2**, 166–186.

Personne, P., Duroure, C. & Isaka, H. 1990 A theoretical study of air inclusions on rotating cylinders. In *Proc. 5th Int. Conf. on Atmospheric Icing of Structures, Tokyo.*

Poots, G. & Skelton, P. L. I. 1990 Theoretical models of rime and glaze accretion with application to freezing rain accretion on overhead transmission line conductors. In *Proc. 5th Int. Conf. on Atmospheric Icing of Structures, Tokyo.*

Roebber, P. & Mitten, P. 1987 Modelling and measurement of icing in Canadian waters. Canadian Climate Centre Report 87-15.

Romagnoli, R. 1988 Ice growth modelling for icing control purposes of offshore marine units employed by the petroleum industry. In *Proc. Int. Association for Hydraulic Research Symposium on Ice, Sapporo*, pp. 486–497.

Ryerson, C. 1995 Superstructure spray and ice accretion on a large US Coast Guard Cutter. *Atmos. Res.* **36**, 321–337.

Sarpkaya, T. & Isaacson, M. 1981 *Mechanics of wave forces on offshore structures.* New York: Van Nostrand Reinhold.

Shellard, H. C. 1974 The meteorological aspects of ice accretion on ships. WMO Marine Science Affairs Report no. 10 (WMO no. 397).

Stallabrass, J. R. 1979 Icing of fishing vessels: An analysis of reports from Canadian east coast waters. National Research Council Canada, Laboratory Technical Report no. LTR-LT-98, Ottawa.

Stallabrass, J. R. 1980 Trawler icing: a compilation of work done at NRC. National Research Council, Mechanical Engineering Report no. MD-56, NRC no. 19372, Ottawa.

Szilder, K. 1993 The density and structure of ice accretion predicted by a random walk model. *Q. Jl R. Met. Soc.* **119**, 907–924.

Szilder, K. 1994 Simulation of ice accretion on a cylinder due to freezing rain. *J. Glaciology* **40**, 180–184.

Szilder, K. & Lozowski, E. P. 1994*a* Stochastic modelling of icicle formation. *J. Offshore Mechanics Arctic Engng* **116**, 180–184.

Szilder, K. & Lozowski, E. P. 1994*b* An analytical model of icicle growth. *Ann. Glaciology* **19**, 141–145.

PHILOSOPHICAL TRANSACTIONS OF THE ROYAL SOCIETY A MATHEMATICAL, PHYSICAL & ENGINEERING SCIENCES

Szilder, K. & Lozowski, E. P. 1995*a* A new method of modelling ice accretion on objects of complex geometry. *Int. J. Offshore Polar Engng* **5**, 37–42.

Szilder, K. & Lozowski, E. P. 1995*b* Experimental verification of a pendant ice formation model. In *Proc. 5th Int. Offshore and Polar Engineering Conf.*, vol. II, pp. 469–475.

Szilder, K. & Lozowski, E. P. 1995*c* Simulation of icicle growth using a three-dimensional random walk model. *Atmos. Res.* **36**, 243–249.

Szilder, K., Lozowski, E. P. & Gates, E. M. 1987 Modelling ice accretion on non-rotating cylinders—the incorporation of time dependence and internal heat conduction. *Cold Regions Sci. Technol.* **13**, 177–191.

Tabata, T., Iwata, S. & Ono, N. 1963 Studies of ice accumulation on ships. Part I. *Low Temperature Sci.* A **21**, 173–221.

Wise, J. A. & Comiskey, A. L. 1980 Superstructure icing in Alaskan waters. Contribution no. 468 from NOAA/ERL Pacific Marine Environmental Laboratory, Seattle, WA, NOAA Special Report.

Zakrzewski, W. P. 1987 Splashing a ship with collision-generated spray. *Cold Regions Sci. Technol.* **14**, 65–83.

Zakrzewski, W. P. & Lozowski, E. P. 1987 The application of a vessel spraying model for predicting ice growth rates and iceloads on a ship. In *Proc. 9th Int. Conf. on Port and Ocean Engineering under Arctic Conditions*, vol. 3, pp. 591–603.

Zakrzewski, W. P. & Lozowski, E. P. 1991 Modelling and forecasting vessel icing. In *Freezing and melting heat transfer in engineering* (ed. K. C. Cheng & N. Seki), pp. 661–706. New York: Hemisphere.

Zakrzewski, W. P., Lozowski, E. P. & Muggeridge, D. 1988 Estimating the extent of the spraying zone on a sea-going ship. *Ocean Engng* **15**, 413–430.

Zarling, J. P. 1980 Heat and mass transfer from freely falling drops at low temperature. US Army Cold Regions Research and Engineering Laboratory, CRREL Report 80–18.